Hall A Annual Report 2014

Edited by Mark M Dalton

Hall A Annual Report 2014

M.M. Dalton[1], E. Chudakov[1], J. Gomez[1], D. W. Higinbotham[1], C. Keppel[1], R. Michaels[1], L. Myers[1], K. Aniol[2], S. Iqbal[2], N. See[2], J.R. Arrington[3], M.V. Ivanov[4,5], M. Mihovilovič[6], S. Širca[6], N. Muangma[7], Dien Nguyen[8], R. Pomatsalyuk[9], O. Glamazdin[9], V. Vereshchaka[9], S. Riordan[10], T. Su[11], V. Sulkosky[12], P. Zhu[13] and the Jefferson Lab Hall A Collaboration[1]

[1]Thomas Jefferson National Accelerator Facility, Newport News, VA 23606, USA
[2]California State University Los Angeles, Los Angeles, CA 90032, USA
[3]Argonne National Laboratory, Argonne, IL 60439, USA
[4]Institute for Nuclear Research and Nuclear Energy, Sofia 1784, Bulgaria
[5]Universidad Complutense de Madrid, Madrid E-28040, Spain
[6]University of Ljubljana, SI-1000 Ljubljana, Slovenia
[7]Massachusetts Institute of Technology, Cambridge, MA 02139, USA
[8]University of Virginia, Charlottesville, VA 22901, USA
[9]National Science Center Kharkov Institute of Physics and Technology, Kharkov 61108, Ukraine
[10]Stony Brook University, Stony Brook, NY 11794, USA
[11]Kent State University, Kent, OH 44240, USA
[12]Longwood University, 201 High Street, Farmville, VA 23909, USA
[13]University of Science and Technology of China, Hefei 230026, People's Republic of China

April 26, 2015

Contents

1 Introduction **6**

2 Hall A Equipment **8**
- 2.1 Hall A BCM System Status . . . 8
  - 2.1.1 Unser Status . . . 9
  - 2.1.2 New BCM receiver test . . . 9
  - 2.1.3 BCM/BPM Fast Readout for Hall A DAQs (in progress) 10
- 2.2 Status of the Hall A Møller Polarimeter Upgrade . . . 14
  - 2.2.1 Conclusion . . . 17
- 2.3 Elastic study of Target boiling effect . . . 20
  - 2.3.1 Introduction . . . 20
  - 2.3.2 Elastic scattering . . . 20
  - 2.3.3 Simulation . . . 21
  - 2.3.4 Outlook . . . 22
- 2.4 ARC Energy Measurement . . . 23

3 Future Experiments **26**
- 3.1 E14009: Ratio of the electric form factor in the mirror nuclei ^{3}He and ^{3}H . . . 26
  - 3.1.1 Experimental Layout . . . 26
  - 3.1.2 Anticipated Results . . . 27
- 3.2 Super Bigbite Spectrometer (SBS) . . . 29
  - 3.2.1 Overview . . . 29
  - 3.2.2 Instrumentation Progress . . . 29

4 Summaries of Experimental Activities **33**
- 4.1 E05102: Double polarized asymmetries in quasi-elastic processes $^3\vec{\mathrm{He}}\,(\vec{\mathrm{e}},\mathrm{e}'\mathrm{d})$ and $^3\vec{\mathrm{He}}\,(\vec{\mathrm{e}},\mathrm{e}'\mathrm{p})$ . . . 33
  - 4.1.1 Introduction . . . 33
  - 4.1.2 The deuteron channel . . . 33
  - 4.1.3 The proton channels . . . 33
- 4.2 E07006: Short Range Correlations (SRC) . . . 37
- 4.3 E08009: $^4He(e,e'p)^3H$ Cross Sections up to $P_{miss} = 0.632GeV/c$ 40
  - 4.3.1 Introduction . . . 40
  - 4.3.2 Experimental cross sections . . . 40
  - 4.3.3 Theoretical cross sections . . . 40
- 4.4 E08027: A Measurement of G_2^P and the longitudinal-transverse spin polarizability . . . 45
  - 4.4.1 Motivation . . . 45
  - 4.4.2 The Experiment . . . 45
  - 4.4.3 Experimental Progress . . . 46

5 Publications **50**

6 Theses **51**

7 Hall A Collaboration Member List, 2014 **52**

List of Figures

1 BCM: The Hall A beam current monitor system. 8
2 BCM: Scatter plot and histogram of Unser output offset. 9
3 BCM: Unser wire calibration. 10
4 BCM: New and old BCM receiver calibration. 11
5 BCM: Event mode operation diagram. 11
6 BCM: Parity mode operation diagram. 12
7 Moller: Møller events shift on the aperture detector 14
8 Moller: Møller dipole shielding. 15
9 Moller: Beam shift after the dipole. 16
10 Moller: Møller DAQ's comparison. 17
11 Moller: Beam energy and position strip-chart. 19
12 Boiling: Simulation Density profile for gas $He4$ Target 20
13 Boiling: Elastic peak check from run 4074, experiment E08-014 . 21
14 ARC: The deviation from the mean of the 8 dipoles in the Hall A ARC 23
15 ARC: The relations between the field integral and current for the 9th magnet mapper dipole. 24
16 E14009: Setup for E14009. 26
17 E14009: Custom collimator plate. 27
18 E14009: Anticipated results. 28
19 E05102: Schematic of $^3\vec{\mathrm{He}}\,(\vec{\mathrm{e}},\mathrm{e'd})$ 34
20 E05102: Asymmetries in quasi-elastic $^3\vec{\mathrm{He}}\,(\vec{\mathrm{e}},\mathrm{e'd})$ 35
21 E05102: Distribution of measured $^3\vec{\mathrm{He}}\,(\vec{\mathrm{e}},\mathrm{e'p})$ events 36
22 E07006: Recoil Proton Momentum Distribution. 38
23 E07006: Semi-Inclusive Ratios. 39
24 E08009: Data compared to full Madrid theoretical calculations. . 41
25 E08009: Data compared to full Madrid theoretical calculations. . 42
26 E08027: Kinematic coverage during the experimental run period. 46
27 E08027: Installation of the g_2^p experiment. 46
28 E08027: Match in focal plane for acceptance study 48
29 E08027: Dilution factor for the 3.35GeV beam energy 49

1 Introduction

contributed by C. Keppel.

The year 2014 welcomed the first 12 GeV era beam back to Hall A in two run periods. While there were challenges to address starting up, both for accelerator and for the Hall, all necessary systems were commissioned, and even a bit of physics data was obtained. Hall A Experiments E12-06-114, a measurement of deeply virtual Compton scattering (DVCS), and E12-07-108, a measurement of the proton magnetic form factor G_M^p, were the first to receive beam in the 12 GeV era. This would not have been possible without the diligent and expert preparatory work of the Hall A collaboration and staff, and the E12-06-114 and E12-07-108 collaborations. All are to be congratulated!

All detector upgrades to both HRSs were highly successful, as was the implementation of the DVCS standalone calorimeter and trigger. The hall beamline was largely commissioned, including the Moller polarimeter, the Hall A arc, a new raster system, the revived Unser, as well as the beam position and charge monitors. The Hall suffered from the loss of the HRS-right front quadrupole magnet, which will be repaired or replaced in 2015. The year ended with work still underway on the harps and the Compton polarimeter.

The 12 GeV scientific plans for the hall consist of many compelling experiments to utilize the standard Hall A equipment, some with slight modifications, in conjunction with the higher energy beam. Four (two newly approved this year) require a ^{3}H target, one to measure the F_2^n/F_2^p structure function ratio at large x, and one to continue the successful Hall A studies of short range correlation phenomena. This target and associated systems are in design currently for a run after the E12-07-108 and E12-06-114 experiments. Beyond experiments that will utilize the standard Hall A equipment are ambitious plans involving multiple new experiment installations.

Construction continued this year on one of these larger scale installation experiments, the Super Bigbite Spectrometer (SBS) program. The SBS project consists of a set of three form factor experiments centered around somewhat common equipment and new experimental capabilities, as well as a semi-inclusive experiment focused on quark transverse momentum dependent distributions. The primary SBS spectrometer magnet was delivered from the Brookhaven National Laboratory, modified, and assembled in the Jefferson Lab test lab. Progress was also made on the detector systems, including GEM trackers and hadron and electron calorimeters. A host of scientific development activities for the program are underway, including detector prototype and construction projects, data acquisition upgrades, and refined physics projections.

Work has continued effectively as well on many other fronts, including infrastructure improvements in data acquisition, offline analysis, and core hall capabilities. Technical preparations are underway for planned experiments such as A_1^n, APEX, CREX, PREX-II, and others. In addition to these, three new experiments were approved this year. Two, mentioned above, will round out the ^{3}H run group and include a measurement of the electric form factor in the

mirror nuclei ^{3}He and ^{3}H and a measurement of the proton and neutron momentum distributions in these nuclei. The third newly approved experiment is a measurement of the spectral function of ^{40}Ar through the (e, e 2p) reaction which is of particular interest to upcoming neutrino experiments.

Looking farther into future planning, the MOLLER experiment had a highly successful Science Review by the DOE this year. Building on the momentum created by the positive review, the collaboration has further developed the intricate spectrometer design, simulated radiation backgrounds, and progressed plans for the beam line and detector systems. The SOLID experiment submitted a Conceptual Design Report for an anticipated 2015 Directors Review. This document is substantial, and reflects excellent work by the collaboration, advancing a highly rated experimental program supported by a well-considered, sophisticated detector system. Plans for the future configuration of the Hall to accommodate first the SBS era, followed by MOLLER and SoLID eras, were made. From these, infrastructure work to accommodate these experiments can commence.

There has been active engagement in analyses of past experiments. Here, fourteen new publications related to Hall A experiments were authored by members of the Hall A collaboration, which included a Physical Review Letter edition with three Hall A articles. In addition, two new Hall A related doctoral theses were successfully defended.

In all, this has been a year of sometimes frustrating, sometimes rewarding, always demanding, work as the first beam was delivered back to the Hall. It continues to be a joy and a privilege to work with the dedicated Hall A community. Please accept my profound thanks to you all for your expert, industrious, innovative efforts. I look forward to continuing the outstanding Hall A program into the 12 GeV era with you!

2 Hall A Equipment

2.1 Hall A BCM System Status

[1]R. Pomatsalyuk, [1]O. Glamazdin, [2]J. Gomez, [2]R. Michaels, [2]L. Myers
[1]National Science Center Kharkov Institute of Physics and Technology, Kharkov 61108, Ukraine
[2]Thomas Jefferson National Accelerator Facility, Newport News, VA23606, USA

The Hall A beam current monitor system consist of two cavity monitors and a parametric current transformer (PCT, "Unser"). It is designed to measure a continues electron beam (∼500 MHz pulse rate). The schematic diagram of Hall A beam current monitor system is shown on Fig. 1. Two cavity monitors "Upstream" and "Downstream" are calibrated with respect to a Faraday Cup. The Unser is an absolute measuring device but it suffers of offset drifts equivalent to a couple of μA [1]. Its calibration can be checked periodically by injecting a known current through a wire crossing the Unser toroid parallel to the beam direction.

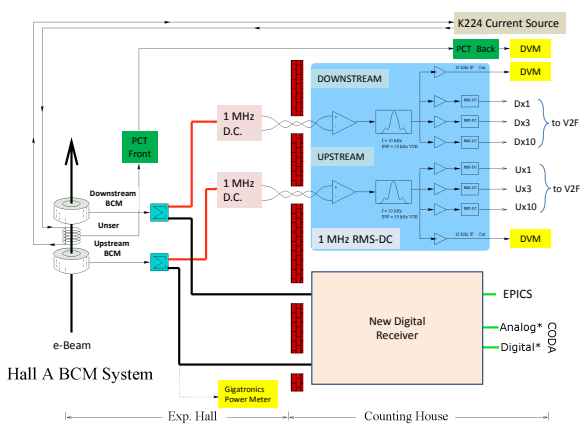

Figure 1: The Hall A beam current monitor system.

In the past a two stage calibration procedure was used:

- linearity test of the Hall A BCM cavities with respect to the **Faraday Cup #2**;
- cross calibration of the Hall A Unser monitor with the **Faraday Cup #2**.

The cavity monitor signal is split and sent through two parallel paths. One path leads to the old 1 MHz electronic box and another one is connected to a new digital receiver [2]. The AC output of 1 MHz electronic blocks is connected to a digital voltmeter (DVM) with EPICS readout. Three voltage-to-frequency

converters (VtoF) per cavity provide a value of the instantaneous beam current to the DAQ system. Three VtoF converters are used to maximize the dynamic range.

New digital receiver has FPGA logic on board and digital signal processing (flexibility to be customized for our goals). It has also analog output from DAC (18 bits, compatible with old system) and digital interface (TTL, optical) for fast data transfer. The new digital receiver can be used also with beam position monitor (BPM). In that case it provides measure of an electron beam position.

More information about Hall A BCM/Unser can be found on the web-page.[1]

2.1.1 Unser Status

As it was mentioned before, the Unser has offset drifts order of ± 2 μA rms at constant temperature and a slope of ± 5 $\mu A/°$C that cannot be compensated in place. These numbers are not determined by the electronics but by the magnetic material used to build the sensor head (Vitrovac®6025) [3]. An example of the Unser drifts taken during a 24 hours period at 5 sec sampling interval is shown on Fig. 2.

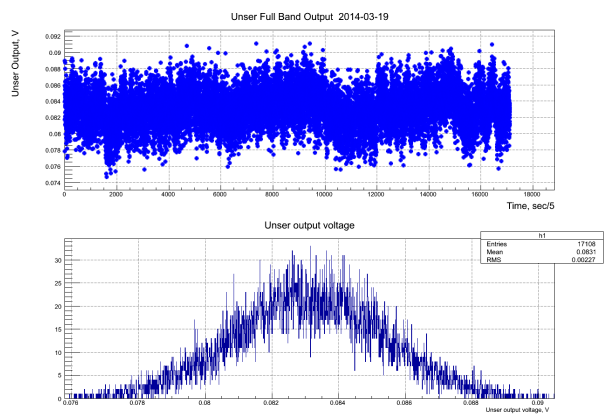

Figure 2: Scatter plot (top) and histogram (bottom) of Unser output offset measured during 24 hours (with 5 sec time interval).

2.1.2 New BCM receiver test

New digital BCM receiver was installed on November 2014 in the Hall A. The result of linearity test of both the new digital BCM receiver and the old 1 MHz BCM receivers with RF current source performed by J. Musson and L. Myers are shown on Fig. 4. [2] Both systems appear to be quite linear (the residuals are less than 1% above 1 μA). The new receivers are linear up to 30 μA. The

[1] http://hallaweb.jlab.org/equipment/BCM/
[2] HALOG entry #3306142

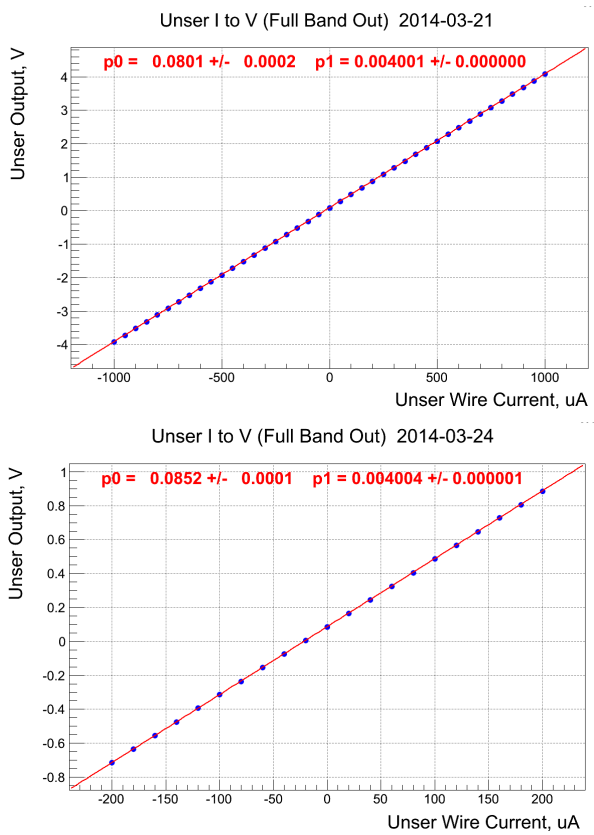

Figure 3: Unser wire calibration with current source K224 for different ranges.

observed saturation at higher beam current (100 μA) was due to the chosen electronic gain. The gain can be changed to work at higher current.

2.1.3 BCM/BPM Fast Readout for Hall A DAQs (in progress)

A fast readout of the beam current monitor and position monitor via the new digital receiver system is being develop. Here we summarize the requirement we are working to meet. Two modes of operation are considered,

Event mode

An event is a moment in time defined by a trigger from detectors. Events arrive randomly in time (see Fig. 5).

- A snapshot of the BPM data, ideally with 5 μm resolution (RMS of distribution) and integrated over a time interval δt which is smaller than *1/fraster* or *1/fmovement*. Here, *fraster* is the raster frequency (25 kHz) and *fmovement* is the (presumably low) frequency of other movements of the beam. So, ideally $\delta t \leq 4$ μsec; if there is a phase lag of a few μsec between the raster and the data, because this could be calibrated out.

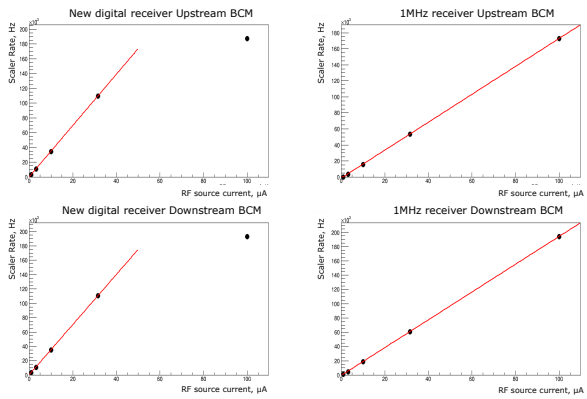

Figure 4: The calibration of new digital BCM receiver (left) and old 1 MHz BCM receiver (right) with RF source.

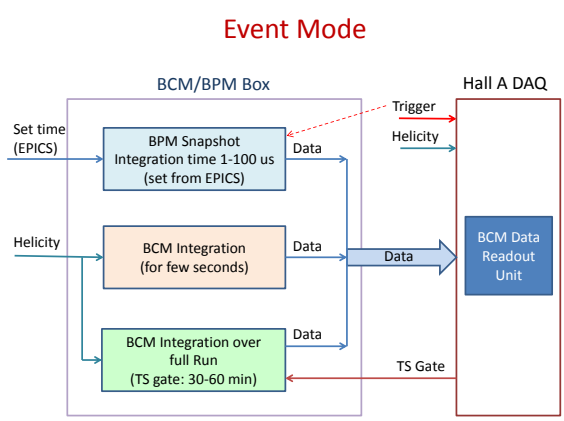

Figure 5: Event mode operation diagram.

- Other experiments could pick a longer integration time to achieve a higher accuracy per snapshot. It is recommended to let δt be a control parameter which would be set infrequently, like maybe at the start of an experiment.
- Snapshots of the BCM data with the integration time few seconds.
- The beam charge integrated over the time of a "run". A run lasts 30 to 60 minutes, typically. The time of a run is provided by a logic gate from the Trigger Supervisor (TS Gate).

Parity mode

The DAQ runs at a fixed frequency governed by the helicity control board. Helicity frequency is in range from 30 Hz up to 2 kHz (see Fig. 6).

- BCM (or BPM) signals are integrated over the interval of the helicity (0.5 - 30 ms). In between the helicity flips, there is blank off the integration for typically 100 μsec (MPS) to allow for the Pockels Cell at the polarized source to settle.
- The integration gate can be provided by the Hall A DAQ.

The consumers of the Event Mode are:

- HRS DAQ;
- SBS DAQ;
- Third arm DAQs (e.g. Bigbite).

The consumers of the Parity Mode are:

- HAPPEX DAQ;
- Moller Polarimeter DAQ;
- Compton Polarimeter DAQ.

There could be other DAQ systems that use these data. The BCM data readout unit is supposed to be a custom VME unit to receive serial data stream. The unit is under development.

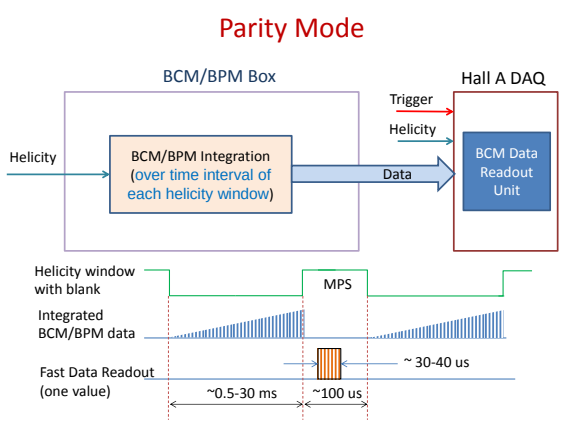

Figure 6: Parity mode operation diagram.

References

[1] J.C. Denard *et al.*, Proceedings of the 2001 Particle Accelerator Conference, Chicago(2001), 2326.

[2] J. Musson *et al.*, Proceeding of 2009 Particle Accelerator Conf.,Vancouver, BC, CA, May 2009.

[3] K.B. Unser *et al.*, Proceedings of the third Beam Instrumentation Workshop, 1991, CEBAF, Newport News, VA.

2.2 Status of the Hall A Møller Polarimeter Upgrade

[1]O. Glamazdin, [2]E. Chudakov, [2]J. Gomez, [1]R. Pomatsalyuk, [1]V. Vereshchaka
[1]National Science Center Kharkov Institute of Physics and Technology, Kharkov 61108, Ukraine
[2]Thomas Jefferson National Accelerator Facility, Newport News, VA23606, USA

The Hall A Møller polarimeter was upgraded in the period 2010 - 2013 in line with the plan to upgrade CEBAF to beam energy of up to 12 GeV. The main purpose of the upgrade was to expand the operating energy range of the Møller polarimeter from $0.8 \div 6.0$ GeV before the upgrade to $1.0 \div 11.0$ GeV after the upgrade [1]. The first commissioning run of the Møller polarimeter after the upgrade was done in April 2014 with a beam energy of 6.05 GeV. The test showed that all elements of the upgraded polarimeter are working properly.

A significant asymmetry of counting rates between the left and right arms of the Møller detector was found while tuning the Møller detector. Analysis of the counting rates indicated that total misalignment of the elements of the polarimeter is up to 10 mm (see Fig. 7).

Figure 7: Left: GEANT-simulated distribution of the Møller events at the aperture detector. Right: amplitude spectra of the signals from the aperture detector measured with the coincidence trigger (both arms aperture and calorimeter detectors in coincidence).

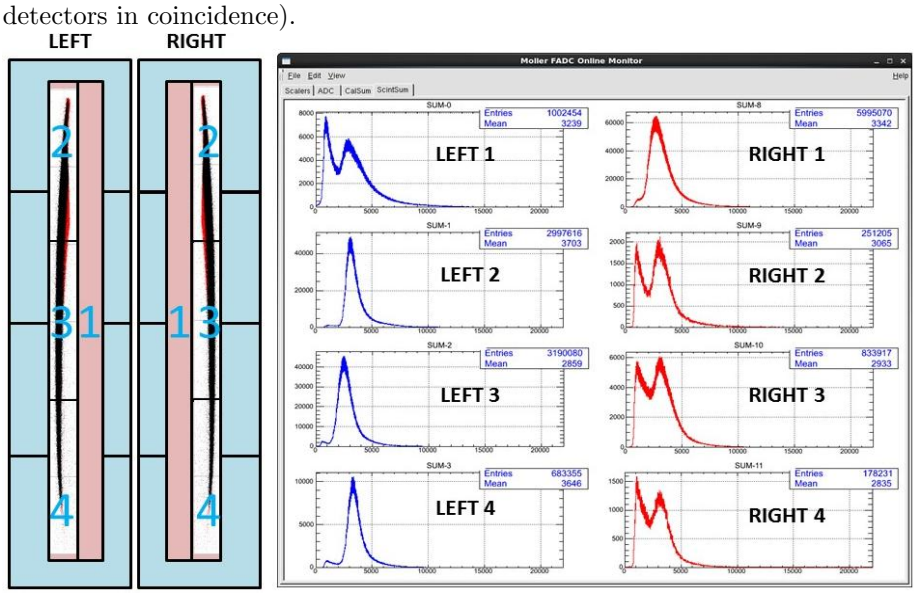

Following the commissioning run, the Møller polarimeter dipole and detector components positioning were checked by the Jefferson Lab Survey and Alignment group. The results are listed below,

- The lead collimator downstream of the Møller dipole magnet was shifted 4.2 mm to the right of the beam axis;
- The slit upstream of the detector was shifted about 1 mm to the right;
- The rectangular slot upstream of the detector shielding box was shifted about 1 mm to the right;
- The center of the detector was 2.5 mm to the left of the beam axis.

Thus, the total measured misalignment of the polarimeter elements was about 8.7 mm. This value is in good agreement with the prediction based on the detector counting rates asymmetry. The largest part of the misalignment - the 4.2 mm shift of the lead collimator was fixed in summer 2014.

Figure 8: TOSCA result for the Møller dipole with the 10 cm extended shielding pipe. A picture of the Møller dipole with additional shielding pipe (left picture). TOSCA calculation of the electron beam shift on the Hall A target (right picture). The beam energy is shown with a red circle.

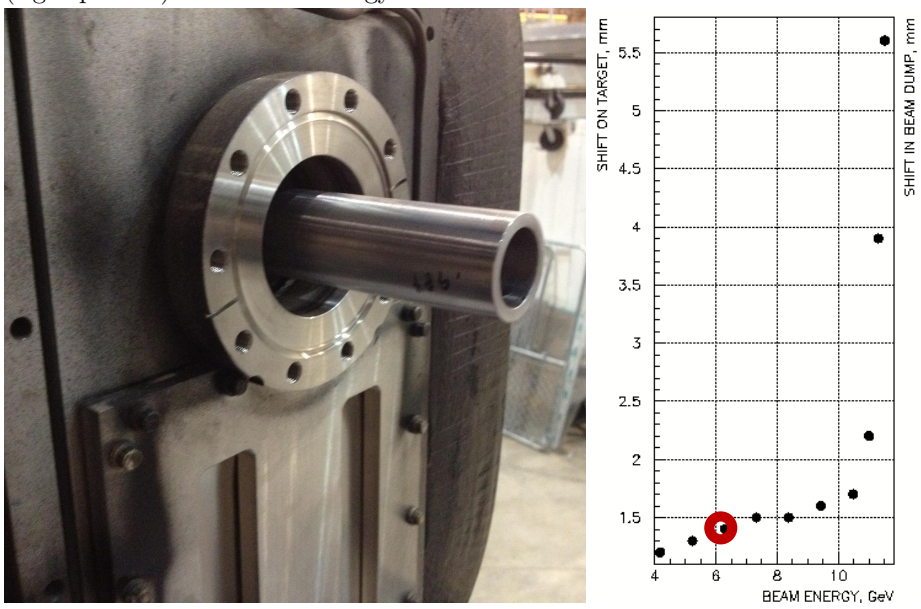

A critical part of the upgrade is a better magnetic shielding of the electron beam line within the dipole magnet. Operations at a higher beam energy require a higher field in the dipole, saturating the existing shielding insertion. A steel pipe was added into the shielding insertion throughout the length of the dipole, extending from its upstream and downstream sides (see Fig. 8). Results of TOSCA calculations of the shielding properties of the Møller dipole magnet

after the upgrade is shown in Fig. 8. The residual magnetic field in the dipole is expected to cause a 1.4 m downward deflection of a 6.05 GeV electron beam at the target location. Fig. 9 shows the electron beam position shift caused by the field in the Møller dipole magnet, in the area close to the target. The shift of about 1.4 mm agrees well with the results of the TOSCA calculations.

Figure 9: Vertical beam shift on the BPM 1H04D downstream of the Hall A Møller polarimeter after the Møller dipole is turned ON.

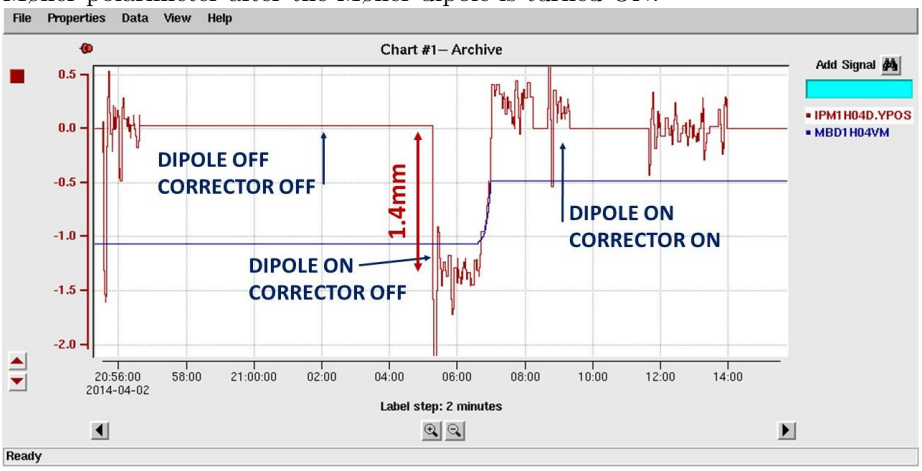

The Hall A Møller polarimeter has two data acquisition and processing systems [2]:

- Old DAQ is based on CAMAC, VME, NIM modules;
- New DAQ is based on VME module Flash-ADC F-250 designed by Jefferson Lab.

Both DAQs are used simultaneously to measure the electron beam polarization. The old DAQ, in operation since 1998, is fully functional but may not be repairable in case of malfunction, as the electronic modules used are not in stock and are not manufactured anymore. The new DAQ based on Flash-ADC, is in operation since 2010, is more precise and provides more detailed data analysis. However, it currently requires more careful adjustment and further improvements. Fig. 10 shows comparison of the asymmetry values measured by both DAQs. Red dots show the measurement result with the new DAQ system based on Flash-ADC, and blue dots show the measurement result with the old DAQ system. The discrepancy between the two DAQs results do not exceed the statistical error[3]

[3]Both DAQ systems collect largely overlapping event samples. The statistical errors should be strongly correlated.

Figure 10: Result of the beam asymmetry measurement with two Møller polarimeter DAQs.

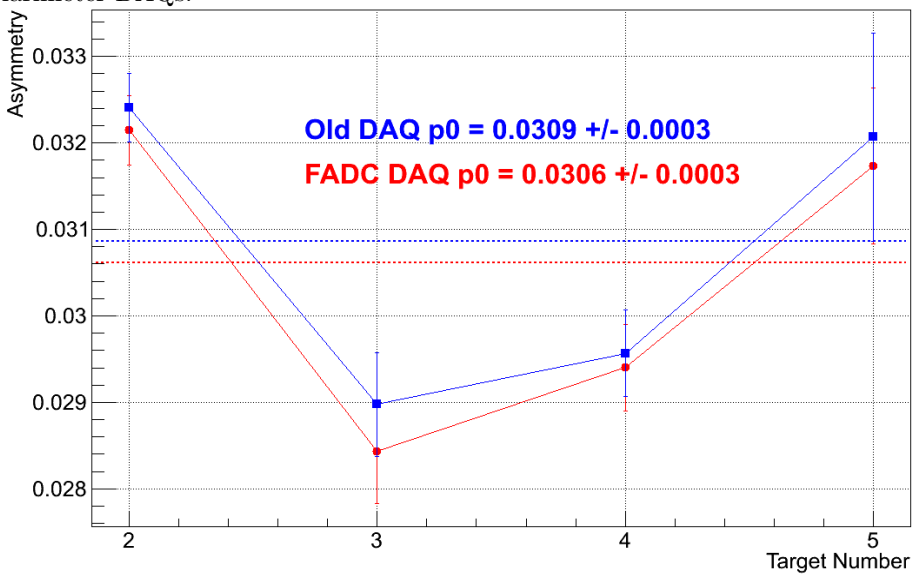

Another beam polarization measurement was done on December 14, 2014. The beam energy was about 7.4 GeV. Unfortunately, the beam energy and position stability was very poor, as it is shown in Fig. 11, in comparison with the typical stability of ± 0.1 mm during the 6 GeV era. Therefore, no additional progress with commissioning of the Hall A Møller polarimeter or studying the systematic errors was possible.

2.2.1 Conclusion

- The Hall A Møller polarimeter is back to operation after the upgrade. Two beam polarization measurements were done in 2014;
- Properties of the new shielding insertion to the Møller dipole magnet look consistent with the TOSCA calculations;
- A misalignment of the Møller polarimeter elements was found and partially fixed;
- Both old DAQ and FADC DAQ are working properly;
- More systematic studies of new polarimeter optics have to be done.

References

[1] O. Glamazdin *et al.*, Hall A Annual report 2012. pp.14-24 (2013). arXiv:1302.4324 [physics.ins-det]

[2] O. Glamazdin *et al.*, Hall A Annual report 2013. pp.8-15 (2014). arXiv:1402.7028 [nucl-ex].

Figure 11: Strip-chart of the beam position stability (on the top) and the beam energy stability (on the bottom) at the time of the beam polarization measurement with the Hall A Møller polarimeter on December 14, 2014.

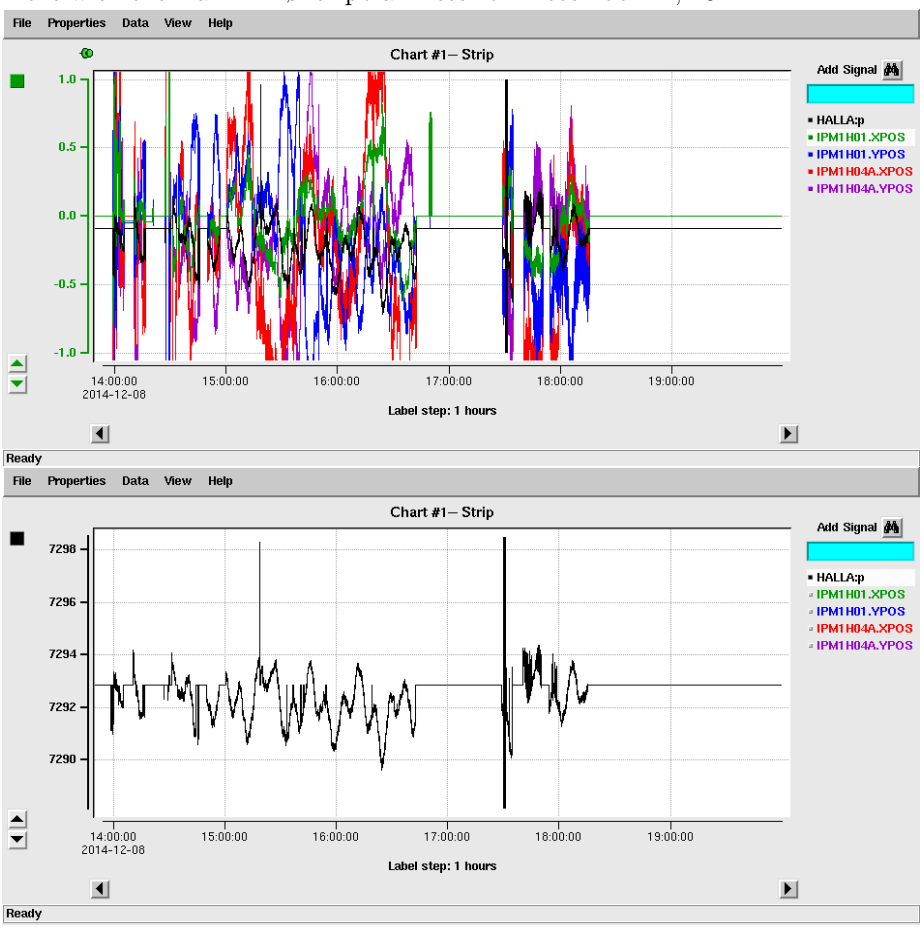

2.3 Elastic study of Target boiling effect

D. W. Higinbotham, Dien Nguyen

2.3.1 Introduction

For cross section extractions, it is very important to know the absolute thickness of the targets. In experiment E08014, we used gas $He3$ and $He4$ targets. From boiling effect studies of these targets, we found large, current dependent target density fluctuations along the target cell. Silviu Covrig simulated this effect using his computational fluid dynamic model and was able to generate a density profile similar to what was seen in the data (see Figure 12),[1]. In order to cross check that we are obtaining the correct absolute thickness, we checked to see if the $3He$ elastic peak was visible in the data for the lowest Q2 in the data set.

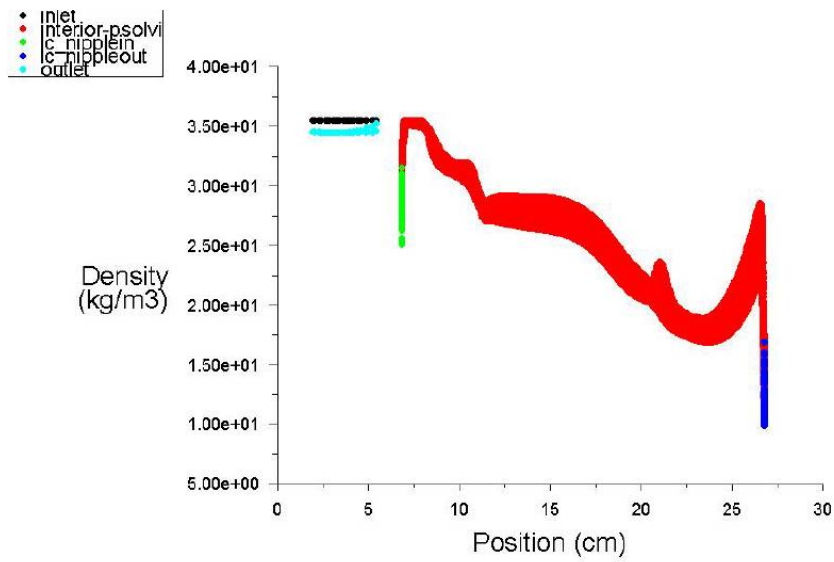

Figure 12: Simulation Density profile for gas $He4$ Target, pressure: $202psia$, current: $120\mu A$

2.3.2 Elastic scattering

Using a well measured reaction channel is often used as a cross check of absolute normalizations.

For 3He, we have both good theoretical calculations and experimental measurements of the form factors and thus good knowledge of the cross sections [2, 3].

Using these results as a references, we have analyzed the elastic study of Target boiling effect for elastic scattering events (see Figure 13 and [1]).

The elastic data is from runs with beam energy of 3.356 GeV, central scattering angle of 21 degrees, and central momemtum of 3.055 GeV. Even with this high energy and large angle, we were still able to clearly identify the elastic peak using cuts on Cherenkov, target vertex, trigger type, solid angle, and reaction point.

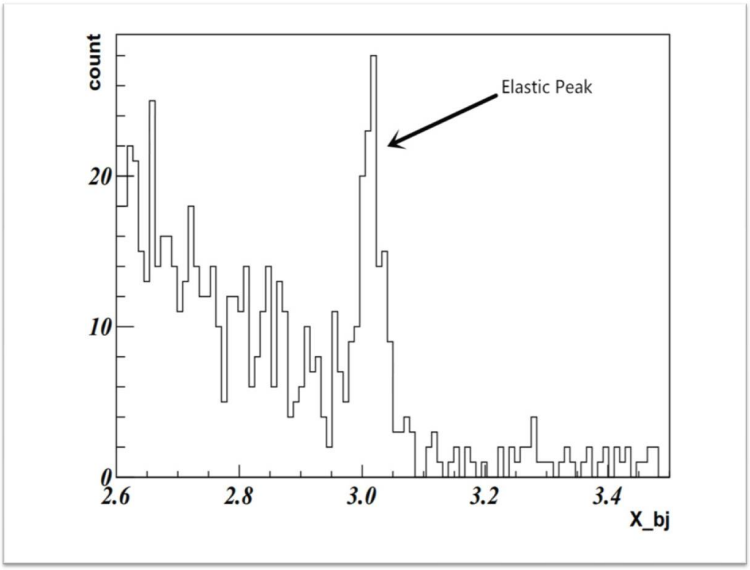

Figure 13: Elastic peak check from run 4074, experiment E08-014, $E0 = 3.356$ GeV, $\theta = 21$ degrees

2.3.3 Simulation

Using the MCEEP simulation, we simulated the $3He$ elastic scattering and applied the same cuts as were used in the data analysis.

To check that the code was working correctly, we first simulated a point target and checked the result against a hand calculation and got good agreement. Then to mimic the density profile, we took the extended target and broke it into 4 sections with different densities and calculated the yield for each section. This of course can be repeat for a large number of sections (i.e. a finer grid of densities). The total yield is simply the sum of these yields. After that we applied the radiative correction to total yield and compared to the yield of real data.

From the real data, one run yield is about 185 events. We have five runs we can use to see the elastic peak and thus we expect to be able to extract about 1000 elastic events and thus we should be able to check the E08-014 density to

the three percent level.

Thus far, the results seem to be in reasonable agreement; but we still need to work the efficiency corrections which thus far are still preliminary.

2.3.4 Outlook

We should be able to use this same technique to get check the target densities for the upcoming tritium experiments. With very first approximation the result look very promising.

From simulation, we find that a run with an angle of 12 and 15 degrees, beam energy of 2.2 GeV and a beam current of $25\mu A$, active length of the target of 20cm would only need $\approx$ 1 hour of beam to achieve less then one percent uncertainty (see table1). Thus, we should be able to check the target thickness of the tritium target to the 1-2 percent level.

Table 1: Yields and Statistic Errors in Percent

Target	Angle1	Angle2	Yield1	Yield2	Uncertainty1	Uncertainty2
$He3$	12	15	3e6	1.7e5	0.05	0.16
$H3$	12	15	4e5	1.9e4	0.24	0.72

References

[1] Silviu Covring, "Private communication"

[2] J. S. McCarthy, I. Sick, R. R. Whitney, "Electromagnetic structure of the helium isotopes" Phys. Rev. C **15, number 4**, 1396-1414 (1976).

[3] I. Sick, "Model independent nuclear charge densities from elastic electron scattering", Nuclear Physics **A218**, 509-541 (1974).

2.4 ARC Energy Measurement

contributed by Tong Su and D. Higinbotham

The ARC energy method uses a dipole magnet mapping system which is connected to a 9th dipole in series with the 8 dipoles in the ARC along with beam position information to determine the CEBAF electron beam energy. Since the energy upgrade in the Hall A, the excitation current range for the dipoles has been extended and all of the dipole were refurbished. Thus for the 12GeV era, dipoles need to re-calibrated and the beam energy vs. ARC current set points needs to be redetermined.

The absolute field in the 9th dipole is calibrated using a NMR probe and the field integral is be determined with coils mount on a translation table that moves the coils through the magnetic field at a known velocity. The field integral of the nine dipoles has been measured w.r.t to the 8 dipoles down in the ARC. The field integral difference of the 8 ARC dipoles at currents 270A, 405A, 540A is shown in Fig. 14.

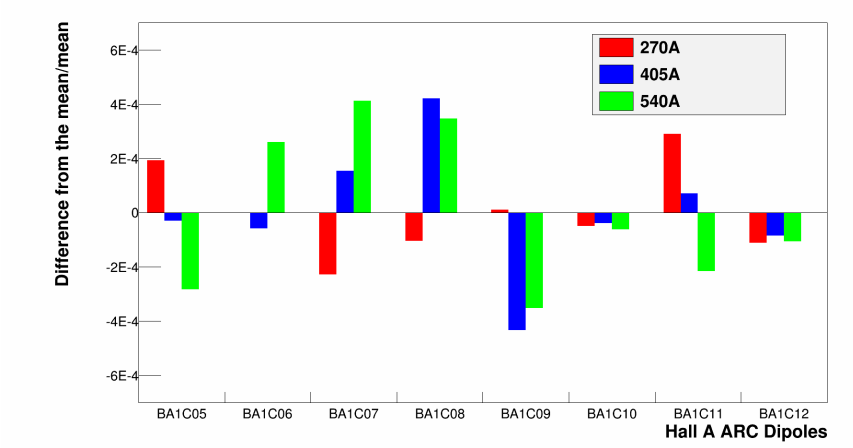

Figure 14: The deviation from the mean of the 8 dipoles in the Hall A ARC.

For the 9th dipole, field integral at the full excitation current range(up to 570A) has been measured and as one can see in Fig. 15 at the highest excitation currents the magnet is starting to saturate as can be seen from the field vs. current has deviating from linearity.

To make sure that the set current of accelerator is equal to the true current in the dipoles, we have installed a calibrated Ultrastab Saturn unit with a 2000A head. With this unit in place, we found an issue with the calibration constant that was being used by the IOC reporting the ARC current. Once this was fixed in late December, the current set by accelerator and our independent Ultrastab measurements have agreed at better then the 1E-4 level.

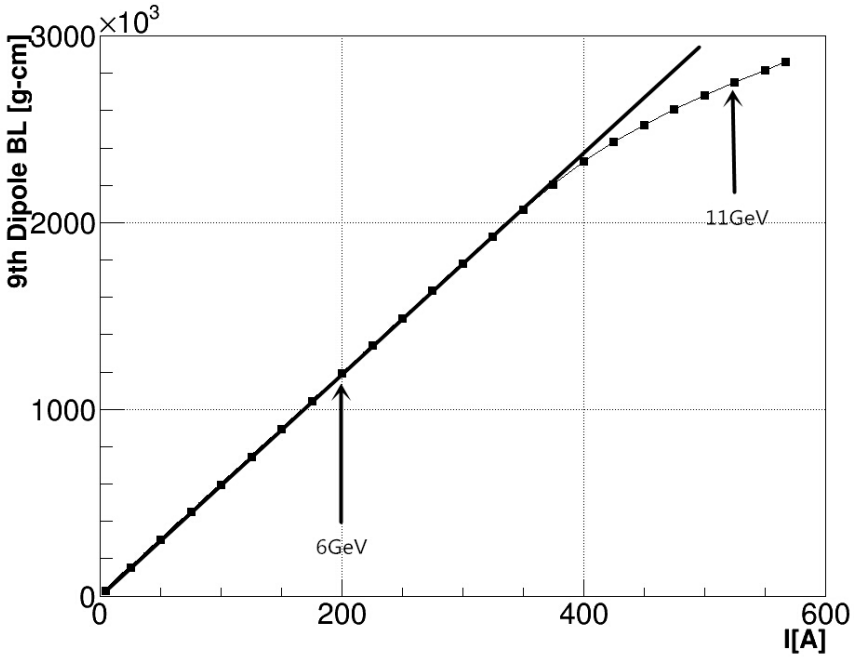

Figure 15: The relations between the field integral and current for the 9th magnet mapper dipole.

Using the 9th dipole and its relation to the other 8 dipoles allows one to determine the field integral of the dipoles in the ARC. Combining this information with the bending angle from the Hall A scanners, one can determine the absolute energy to the $5x10^{-4}$ level. By changing ARC tune to a fully dispersive mode, instead of its normal tune and using the super-harps to determine the deflection angle this precision can be pushed to the few 10^{-4} level. In the future, we will compare the results of the ARC energy measurements with the energy determined using spin precession [2, 3].

We do note that in order to get the precise energy for the beam on target, for both these measurement techniques the synchrotron needs to be taken into account. To do this precisely, we have been working with Yves Roblin who within the context of his model of the accelerator can precisely calculate that correct for the exact geometry of the accelerator.

References

[1] F. Kircher et al., High Accuracy Field Integral Measurement for CEBAF Beam Energy determination, submitted to MT16 Conference, Jacksonville, Florida (USA) (Sept. 1999.)

[2] J. M. Grames *et al.*, "Unique electron polarimeter analyzing power comparison and precision spin-based energy measurement," Phys. Rev. ST Accel. Beams **7**, 042802 (2004) [Erratum-ibid. **13**, 069901 (2010)].

[3] D. W. Higinbotham, "Electron Spin Precession at CEBAF," AIP Conf. Proc. **1149**, 751 (2009) [arXiv:0901.4484 [physics.acc-ph]].

3 Future Experiments

3.1 E14009: Ratio of the electric form factor in the mirror nuclei ^{3}He and ^{3}H

contributed by L. S. Myers, D. W. Higinbotham and J. R. Arrington.

The E14009 experiment [1] proposes to measure the ratio of the electric form factors of ^{3}He and ^{3}H over a range of Q^2 from 0.05 to 0.09 GeV^2. From this measurement, the relative charge radii for the A=3 nuclei can be determined. From this relationship, the experiment plans to extract the charge radius difference with an uncertainty of ∼15% – a significant reduction from the current 50% uncertainty. The JLab PAC42 approved the experiment for the requested 1.5 days of beam time. This experiment will run with at the same time as the other approved triton experiments [2, 3, 4].

3.1.1 Experimental Layout

The experiment will be a single-arm measurement of elastic electron scattering from ^{3}He and ^{3}H (see Fig. 16). It will utilize the left high-resolution spectrometer (LHRS) in Hall A positioned at 12.5° and 15.0°. In general, the setup is very similar to previous form factor measurements in Hall A, as well as the other planned triton experiments.

Figure 16: A schematic diagram of the experimental setup for E14009. Only the left HRS will be employed for this measurement. Targets of ^{1,2,3}H, ^{3}He, and ^{12}C are planned for study. A custom collimator plate (see Fig. 17) will be utilized.

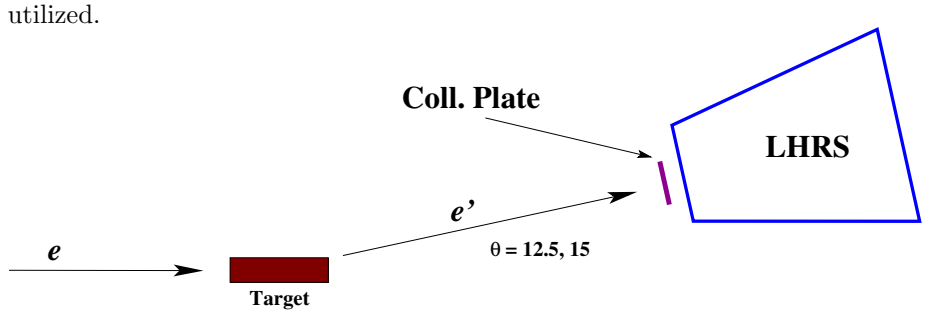

There are two unique features of the setup for E14009. First, the electron beam will be set to 1.1 GeV (the lowest achievable energy with the upgraded accelerator) and the current will be limited to only 5 μA. The energy is necessary to get down to Q^2 of 0.05–0.09 GeV^2. At these momentum transfers, the cross sections and scattering rates are large. The reduced current eliminates the need for a large trigger prescale factor in the data acquisition.

The other unique feature of E14009 is the custom collimator plate (Fig. 17) to be placed on the spectrometer. This plate serves three purposes: (1) the center slot further reduces the event rate in the HRS while (2) the tapered design reduces the rate on the low-angle side thereby balancing the rates in each of the five Q^2 bins, and (3) the rows of holes above and below the center slot allow for in situ optics measurements.

Figure 17: The custom collimator plate for the experiment (not to scale). The bin labeled '1' is the smallest Q^2 point at the given angle setting. The holes above and below the center slot are for simultaneous optics measurements.

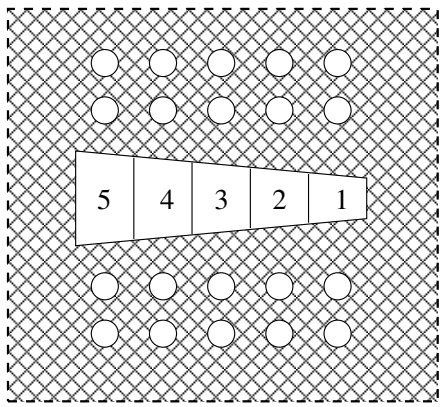

3.1.2 Anticipated Results

The count rates for the elastic electrons are expected to be $\sim 10^5$ counts/hr per Q^2 bin. Data taking for each target will take 1.5 hrs at each HRS angle. As a result, the systematic uncertainties ($\sim$ 2%) will dominate the statistical (<0.5%). Within the systematic uncertainty, the largest contribution is expected to come from the relative thickness of the ^{3}H and ^{3}He targets. This uncertainty ($\sim$1.5-2.0%) will be finalized using deep inelastic scattering from both targets during the running of the MARATHON experiment.

The anticipated results for the experiment are shown in Fig. 18. Assuming a conservative estimate of the uncertainties, the ^{3}He–^{3}H can be determined to $\sim$0.03 fm, a reduction of 70% from the current uncertainty. The model dependence of the radius extraction is constrained by examining the evolution of the form factor ratio over the full range of Q^2.

This measurement will also be able to extract the most precise value of the ^{3}H charge radius by using ^{3}He radii available from isotopic shift measurements [6, 7] and soon from muonic ^{3}He [8]. These combined results will allow for the extraction of the proton and neutron radii in the A=3 nuclei which can be compared to ab initio calculations.

Figure 18: The expected results of the measurement of the charge form factor ratio of ^{3}He and ^{3}H. The ^{3}He radius is fixed to 1.96 fm [5]. The solid line assumes a ^{3}H radius of 1.76 fm with ± 0.03 fm used to calculate the dashed lines.

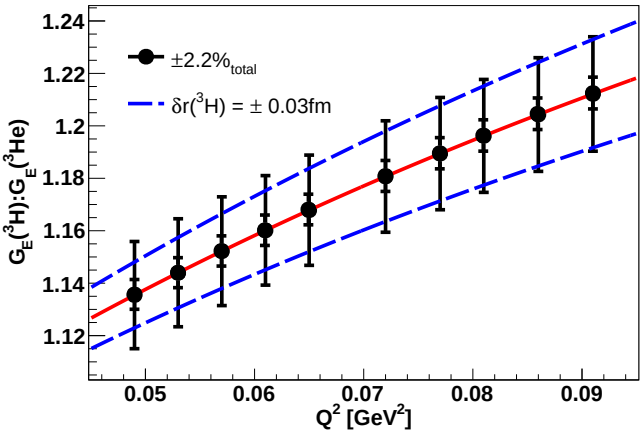

References

[1] L. S. Myers, D. W. Higinbotham, and J. R. Arrington, arXiv:1408.5283 [nucl-ex].

[2] G. Petratos, J. Annand, J. Gomez, R. Holt, R. Ransome *et al.*, Jefferson Lab experiment E12-10-103.

[3] P. Solvignon-Slifer, J. Arrington, D. Day, D. Higinbotham *et al.*, Jefferson Lab experiment E12-11-112.

[4] L. Weinstein, W. Boeglin, O. Hen, S. Gilad *et al.*, Jefferson Lab experiment E12-14-011.

[5] A. Amroun *et al.*, Nucl. Phys. **A579**, 596 (1994).

[6] D. Shiner, R. Dixson, and V. Vedantham, Phys. Rev. Lett. **74**, 3553 (1995).

[7] D. C. Morton, Q. Wu, and G. W. F. Drake, Phys. Rev. A **73**, 034502 (2006)

[8] T. Nebel *et al.*, Hyperfine Interactions **212**, 195 (2012).

3.2 Super Bigbite Spectrometer

Progress by the Super Bigbite Collaboration

contributed by S. Riordan
for the Super Bigbite Collaboration.

3.2.1 Overview

The Super Bigbite (SBS) project is a collection of experiments based upon utilizing large-acceptance single dipole spectrometers designed to operate in a high rate environment in conjunction with the upgraded 12 GeV CEBAF accelerator. The official DOE project of SBS focuses around three coincident nucleon elastic form factor measurements at high Q^2, which require large acceptance but moderate momentum resolution. In addition, there are two approved experiments which also utilize this equipment, making the SBS collaborative effort contain

- E12-07-109, GEp
- E12-09-016, GEn
- E12-09-019, GMn
- E12-09-018, SIDIS
- E12-06-122, A_1^n.

The collaboration underwent a successful annual review of the project in November, meeting the recommendations of the previous review. The full report can be found online [1]. More documentation over the entirety of the project can be found online [2].

3.2.2 Instrumentation Progress

48D48 Magnet and Beamline One critical component of the SBS project is the 48D48 magnet, which serves as the magnetic element for the hadronic arm of these experiments. In the last year, progress was made in completing drawings for the assembly in the SBS configuration, the modification of the iron yoke (completed in May), and the construction of the new racetrack and saddle coils and support platform. The magnet floor layout was changed from beam-left to beam-right to ease installation and compatibility between experiments.

The new racetrack coils have been fabricated and delivered by vendors to Jefferson Lab and underwent local testing. The saddle coil is under construction and is expected to be delivered in July 2015. The power supply was delivered in October and water cooling components were acquired and assembled. A test of the magnet at 200 A was performed and compared to TOSCA simulations with a 2% deviation observed with further studies underway.

In addition, beamline corrector magnets and shielding configurations are under study to compensate for fields as the exit beamline passes through the

magnet iron. The scattering chamber vacuum snout is anticipated to arrive in February with the new consideration of magnet beam-right. Simulations of the background for the shielding has been underway with support of the Yerevan group.

GEM Detectors and Tracking Hardware Several sets of GEM detectors are being constructed by groups at INFN and UVA and will be used in both the hadron and electron arms of these experiments. In 2014 major milestones were completed in the GEM production. The UVA group has received the parts for GEM construction and has now assembled seven modules which are undergoing testing. A high intensity X-ray source has been constructed to provide the capability to do high background testing with rates comparable to SBS conditions.

The INFN collaboration has assembled eight 40×50 cm^2 modules, four of which are undergoing testing with cosmics and HV curing. Short, opportunistic in-beam tests at COSY were performed in December to study the response with a high-intensity proton beam and study HV and gas flow.

A review over the choice of electronics, either the SRS or INFN VME-based MPD APV25 readout systems, was carried out. The MPD system was selected for future use.

The INFN group is also working on the development of two small silicon microstrip planes (10×20 cm^2, 50 μm pitch) to improve the tracking of the primary particles in the front tracker. Evaluation of the response of this system and electronics using a prototype is ongoing and assembly and testing of the detector is expected in 2015.

ECal A primary concern for the electromagnetic calorimeter is the darkening of lead-glass blocks as they absorb radiation and a thermal annealing method which operates continuously has been under investigation at JLab. In 2014 tests were performed quantifying the restoration capabilities using blocks that had been irradiated by Idaho State. The results showed that such a method was feasible but also that when held at a high temperature the optical transparency was slightly reduced. Simulations were performed which quantified the light yield for electromagnetic showers with a transparency gradient to ensure that sufficient resolution would be maintained. A 16-block prototype has been assembled with support from the Yerevan group at Jefferson Lab waiting to undergo testing in the hall when beam is restored in spring using a coincident trigger to select an electron with well defined energy. Stony Brook University has agreed to lead the development of a 200-block prototype with drawings produced with the support of the Yerevan group. This prototype will have the design finalized and constructed in 2015 for the purposes of testing a mechanical and thermal design and costing.

HCal-J The hadronic calorimeter, HCal-J, serves as a primary component in hadron detection for the form factor and SIDIS experiments and is being

constructed at Carnegie Mellon University with contributions of funding and manpower by INFN/Catania. In 2014 a fully working prototype was constructed and tested with cosmics. These tests were compared with detailed Monte Carlo simulations, in particular to ensure sufficient timing resolution required for the G_E^n measurement. Iron, scintillator, and wavelength shifter for the full detector has been received and are undergoing machining and assembly. Design of the light guides to optimize readout is undergoing testing using a three-piece acrylic design and transmission tests with comparisons to simulation are ongoing.

Polarized ^{3}He Target The polarized ^{3}He target is at the heart of the A_1^n, G_E^n, and SIDIS experiments and provides an effective polarized neutron target. For SBS beam currents, a design that includes metal end-cap windows, a convection design, and two laser pumping chambers is being developed at UVA. A target-cell design for for this was selected in October and after fabrication, simulated-beam tests are planned.

Gas Cherenkov A 600 PMT gas Cherenkov detector to be used for electron identification is being developed jointly by collaborators at William and Mary, North Carolina A&T State University, University of Glasgow, and James Madison University. The mirror assembly has been produced by the William and Mary machine shop and the optics configuration has been tested prompting the order of the final mirrors. The pressure vessel design is underway at Jefferson lab. NC A&T are in the procurement process for the PMT array and magnetic shielding. JMU has characterized 600 of 800 PMTs and is grouping them based on gains.

Coordinate Detector A scintillator coordinate detector will serve as a hodoscope to determine the electron position in front of the electromagnetic calorimeter in the G_E^p experiment. The position resolution of such a detector will allow for a much cleaner identification of proton elastic events than by the calorimeter alone by exploiting the specific electron-hadron kinematic correlation. Efforts led by the Idaho State and Saint Mary's group for construction are underway after the completion and testing of a prototype module. In 2014, a sample set of scintillator bars were ordered and procured from the Fermilab extrusion facility and considerations are underway to determine where machining will be done. Full production of the scintillator is expected at the end of February. Sample waveshifting fibers from St. Gobain have been received at Jefferson Lab for testing. Drawings for the support structure have been completed and vendors are being selected for fabrication. Electronics are also undergoing testing using a NINO chip and FASTBUS design for readout.

RICH A RICH detector is included with the SIDIS experiment for PID and work of refurbishment of an existing detector is being led by the University of Connecticut group. The detector has been delivered there from storage at UVA. Detailed representations have been included in the Monte Carlo simulation and

an analysis has been performed in the reconstruction and PID capabilities by the same group.

Timing Hodoscope The Bigbite timing hodoscope consists of 90 600x25x25mm plastic scintillator bars, each equipped with 2 fast PMTs and is necessary for accurate coincident time of flight measurements. Tests performed at Glasgow show that 100 ps timing resolution is possible. The bars and lightguides for its construction have been procured and the lightguides have been glued to the scintillator. Glasgow is also developing a NINO-based frontend amplifier/discriminator for this component, as well as for the GRINCH and coordinate detector.

Software and Simulation The Geant4 and ROOT-based SBS Monte Carlo simulation, `g4sbs`, has undergone a huge amount of development with contributions from many different groups. A full realization of all the detector systems has been incorporated, including a detailed representation of the magnets including field clamps, beamline including shielding and magnetic elements, target chamber, RICH, GRINCH, and ECal. Optical photon processes are included to evaluate light yields and backgrounds in the detector responses. A full evaluation of the trigger rates including background for the three form factor measurements has been performed including the calorimeter responses for various particle types and coincident trigger logic. Plans are underway to incorporate the simulation into the analysis framework to test various reconstruction algorithms on pseudodata. The INFN group has been developing a new neural network-based tracking algorithm in parallel of the existing tree search method and will be incorporated.

References

[1] https://cnidlamp.jlab.org/SBS-experiments/JDocDB/system/files/biblio/2015/02/sbs_review_report_2014_final.pdf

[2] http://hallaweb.jlab.org/12GeV/SuperBigBite/

4 Summaries of Experimental Activities

4.1 E05102: Measurement of double polarized asymmetries in quasi-elastic $^3\vec{\mathrm{He}}\,(\vec{\mathrm{e}},\mathrm{e'd})$ and $^3\vec{\mathrm{He}}\,(\vec{\mathrm{e}},\mathrm{e'p})$

Contributed by M. Mihovilovič and S. Širca.

4.1.1 Introduction

The E05-102 experiment [1] is dedicated to the study of the ^{3}He nucleus by measuring double-polarization (beam-target) transverse and longitudinal asymmetries in quasi elastic processes $^3\vec{\mathrm{He}}\,(\vec{\mathrm{e}},\mathrm{e'd})$ and $^3\vec{\mathrm{He}}\,(\vec{\mathrm{e}},\mathrm{e'p})$ as a function of the missing momentum (p_{miss}). The purpose of this measurement is to challenge the existing predictions on the structure and properties of this three-nucleon system and to provide new constraints for the theoretical models. In particular, the $^3\vec{\mathrm{He}}\,(\vec{\mathrm{e}},\mathrm{e'd})$ reaction is a uniquely sensitive probe of hadron dynamics in ^{3}He and the isospin structure of the underlying electro-magnetic currents, while the proton channels $^3\vec{\mathrm{He}}\,(\vec{\mathrm{e}},\mathrm{e'p})\,\mathrm{d}$ and $^3\vec{\mathrm{He}}\,(\vec{\mathrm{e}},\mathrm{e'p})\,\mathrm{pn}$ give us the ability to precisely study final-state-interactions and nucleon-nucleon correlations. The experiment was performed in Summer 2009 by using the polarized ^{3}He target and a High Resolution Spectrometer (HRS-L) in coincidence with the large-acceptance spectrometer BigBite [2].

4.1.2 The deuteron channel

Because of a cleaner experimental signature and more profound implications on the structure of ^{3}He our efforts have primarily been focused on the analysis of the $^3\vec{\mathrm{He}}\,(\vec{\mathrm{e}},\mathrm{e'd})$ channel, which is now complete and published [3]. The measuremens have been confronted with the state-of-the-art Faddeev calculations and the comparison of the asymmetries shows a fair agreement in terms of their functional dependencies in p_{miss} and ω, but significant discrepancies remain, in particular beyond the quasi-elastic peak.

To ensure a truthful comparison of theory to the data, shown in Fig. 20, a sophisticated algorithm for interpolating and averaging a discrete mesh of theoretical points over the measured kinematic acceptance was developed [4]. Additionally, a stand-alone Monte-Carlo simulation was designed to simulate the physics process under scrutiny. The program considers the cross-sections provided by the theoretical groups, radiative corrections in terms of the peaking approximation and the spectrometer acceptances, defined by their collimator sizes. This simulation gave us the ability to validate the theoretical asymmetries determined by the averaging algorithm and to estimate and correct the effects of bin migration, which arise due to radiative losses.

4.1.3 The proton channels

The analysis of the two proton channels is ongoing. Due to insufficient resolution of the experimental apparatus, the two- and three-body channels in the

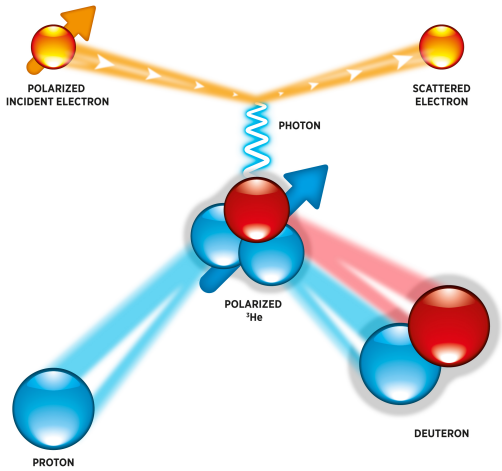

Figure 19: Schematic drawing of the $^3\vec{\mathrm{He}}\,(\vec{\mathrm{e}},\mathrm{e}'\mathrm{d})$ reaction. Longitudinally polarized electrons are scattered off a polarized ^{3}He target. In the process the nucleus breaks up into a proton and a deuteron, which is detected in coincidence with the scattered electron.

proton knockout processes can not be disentangled [5]. Hence, the measured asymmetries are the sums of two reaction processes, which makes the comparison of the data to the simulation much more challenging. To overcome this obstacle, the calculated asymmetries for the two processes at each kinematic point will be weighted by the predicted cross-section and then summed. For the interpolation and averaging of the available theoretical calculations, a similar approach as for the deuteron channel will be employed, but with an additional degree of freedom for the three-body proton breakup, where the $p-n$ system is no longer bound, thus allowing for the final states with different missing energies $E_{\mathrm{miss}} \geq 7.7\,\mathrm{MeV}$ and consequently different asymmetries (see Fig. 21). It is foreseen that this last part of the analysis will be done in 2015 and the results sent to the publication by mid-2016.

References

[1] S. Širca, S. Gilad, D. W. Higinbotham, W. Korsch, B. E. Norum (spokespersons), *Measurement of A_x and A_z asymmetries in the quasi-elastic* $^3\vec{\mathrm{He}}\,(\vec{e},e'd)$, JLab Experiment E05-102, June 2005.

[2] M. Mihovilovič et al., Nucl. Instr. and Meth. A **686** (2012) 20.

[3] M. Mihovilovič et al., Phys. Rev. Lett. **113** (2014) 232505.

[4] M. M. Dalton et al., Hall A Annual Report 2013, arXiv:1402.7028 [nucl-ex].

[5] M. Mihovilovič, PhD thesis, *Measurement of double polarized asymmetries in quasi-elastic processes* $^3\vec{\mathrm{He}}\,(\vec{\mathrm{e}},\mathrm{e}'\mathrm{d})$ *and* $^3\vec{\mathrm{He}}\,(\vec{\mathrm{e}},\mathrm{e}'\mathrm{p})$, University of Ljubljana (2012), arXiv:1208.0748 [nucl-ex].

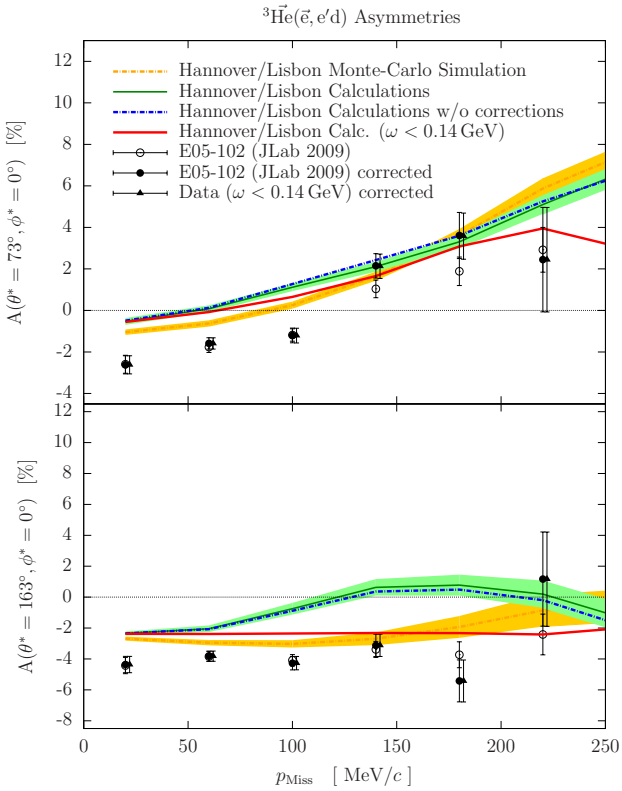

Figure 20: The longitudinal (top) and transverse (bottom) asymmetries in the quasi-elastic process $^3\vec{\mathrm{He}}\,(\vec{\mathrm{e}},\mathrm{e'd})$ as a function of missing momentum (p_{miss}). The empty circles represent data points measured in the E05-102 experiment. Full circles show the same results corrected for the effects of bin migration, which arise due to radiative losses. The full triangles show the measured asymmetries for the events from the vicinity of the quasi-elastic peak ($\omega < 0.14\,\mathrm{GeV}$). The full green line and the blue dash-dotted line show the acceptance averaged theoretical calculations by the Hannover-Lisbon group with and without radiative corrections, respectively. The red line shows the corrected theoretical prediction for the quasi-elastic peak. The yellow dashed line represents the results of a stand-alone Monte-Carlo simulation.

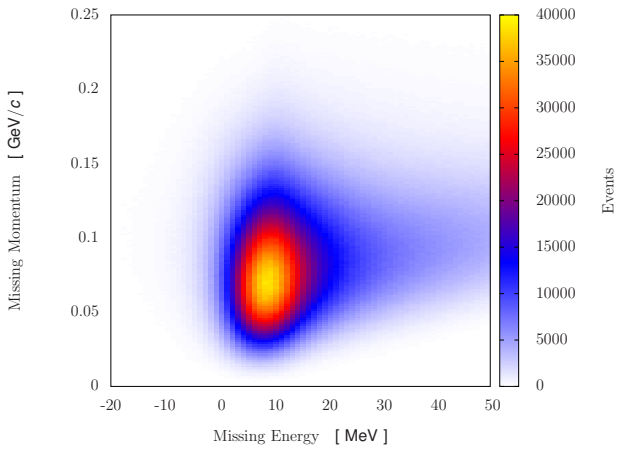

Figure 21: The distribution of measured $^3\vec{\mathrm{He}}\,(\vec{\mathrm{e}}, \mathrm{e}'\mathrm{p})$ events as a function of missing energy (E_{miss}) and missing momentum (p_{miss}). Due to insufficient resolution the two-body breakup peak at $E_{\mathrm{miss}} = 5.5\,\mathrm{MeV}$ can not be separated from the three-body breakup at $E_{\mathrm{miss}} = 7.7\,\mathrm{MeV}$. Additionally, the distribution has a long tail in E_{miss} which needs to be interpreted properly for a objective comparison of the data to the theoretical predictions.

4.2 E07006: Short Range Correlations (SRC)

contributed by N. Muangma and V. Sulkosky

Nucleon-Nucleon Short Range Correlations (NN-SRC) have been studied in both the inclusive reaction $(\mathrm{e}, \mathrm{e}')$ and the exclusive triple-coincidence reaction. For experiment E07-006, we are analyzing two reaction channels: the exclusive reaction $(\mathrm{e}, \mathrm{e}'\mathrm{pN})$ and the semi -inclusive reaction $(\mathrm{e}, \mathrm{e}'\mathrm{p}_{\mathrm{recoil}})$. This experiment is a continuation of the first Hall A SRC experiment, E01-015 [1, 2, 3] by extending the measurement to higher missing momenta. The experimental details and the final results of the exclusive reaction can be found in [4].

The semi-inclusive channel is an attempt to study NN-SRC, in which the statistics are significantly better than the exclusive triple-coincidence reaction. We are exploring if the backward tagged protons, after subtraction of the random background events, are coming from the SRC NN-pair, where the undetected nucleon carried the transferred momentum.

The electrons were detected in the L-HRS, and the recoil protons were detected in the BigBite spectrometer, which was implemented with the hadron detector package [5]. The recoil protons were detected at much larger angle compared to the transferred momentum $\vec{q}$. By using the pion rejectors in the L-HRS, the separation between the pions and electrons was very clean. At this stage of the analysis, we are also extracting the inclusive ratios of the deuteron, ^{4}He and ^{12}C versus x_{bj} to verify that they are consistent the measured a_2 values, where a_2 is related to the number of 2N correlations in the nucleus relative to that of the deuteron.

The backward protons detected in BigBite are identified with the measured momentum from the multi-wire drift chambers (MWDC) and the energy deposited in a pair of scintillator planes, known as the dE and E planes. In principle, the protons can be identified directly from the dE and E planes; however at high momenta, the protons do not deposit enough energy in the dE plane, which requires the use of the the MWDC and the E plane for proton PID.

To obtain the semi-inclusive data above the random background distribution, we are using two coincidence time cuts: the first with a cut on the coincidence time-of-flight (CTOF) peak, and the second with a cut to the sides of the CTOF peak. For the momentum distribution, the random background is estimated from the off-peak CTOF cut. Then the data above background is the data within the CTOF peak subtracted from the estimated random background. Figure 22 shows the six-fold differential cross section versus the proton momentum, which has been corrected for energy losses. The blue data represent the signal and background together, the red shows the estimated background contribution, and the green is the background subtracted distribution.

In case of the semi-inclusive cross-section ratios of nuclei versus x_{bj}, we found a *flat* region starting around 0.9 up to 1.3, which begins below the flat region of the inclusive ratio ($x_{bj} > 1.3$), see Fig. 4.2. The ratio value is not equal to the a_2 value. Further study is required to understand this phenomena.

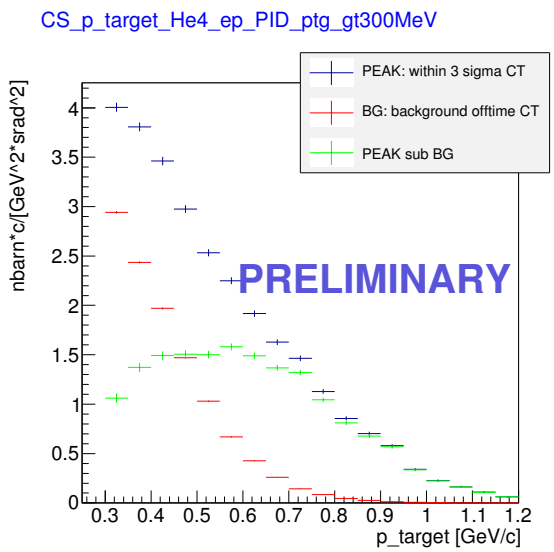

Figure 22: The six-fold differential cross section for the $^4\mathrm{He}(\mathrm{e},\mathrm{e}'\mathrm{p}_{\mathrm{recoil}})$ reaction versus the detected recoil proton momentum, p_{target}. The green data points represent the data after subtraction of the random background.

References

[1] R. Shneor *et al.*, Phys. Rev. Lett. **99** 072501 (2007).

[2] R. Subedi *et al.*, Science **320** 1476 (2008).

[3] P. Monaghan *et al.*, J. Phys. G **41** 105109 (2014).

[4] I. Korover *et al.*, Phys. Rev. Lett. **113** 022501 (2014).

[5] M. Mihovilovic *et al.*, Nucl. Instrum. Meth. A **686** 20 (2012).

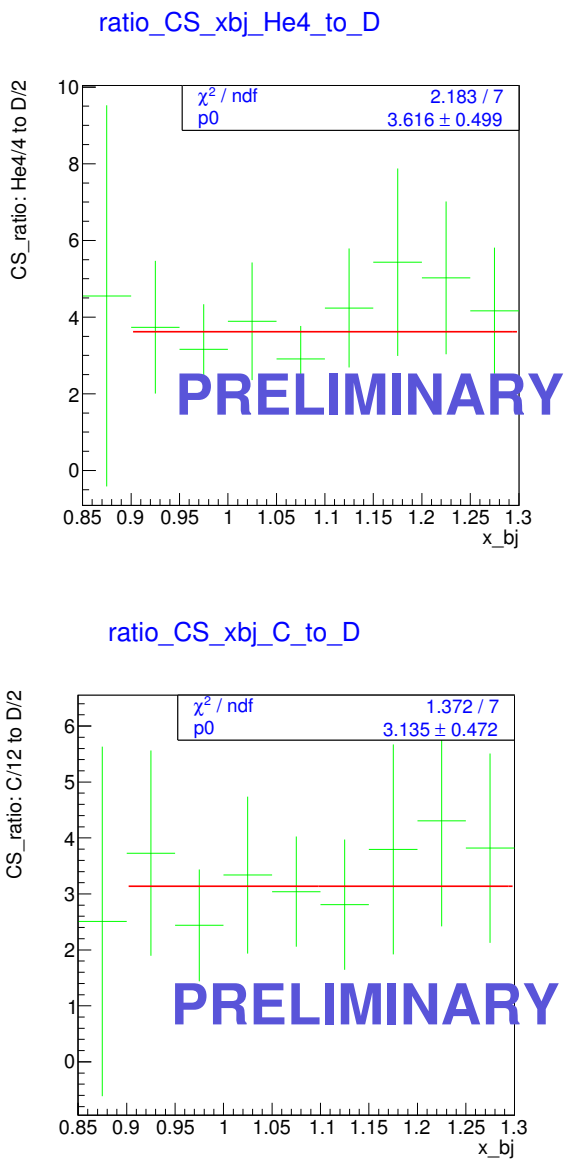

Figure 23: Semi-inclusive cross-section ratios versus x_{bj}. The top panel is the ratio of ^{4}He to deuterium, and the bottom panel is the ratio of ^{12}C to deuterium.

4.3 E08009: $^4He(e,e'p)^3H$ Cross Sections up to $P_{miss} = 0.632 GeV/c$

S. Iqbal, M. Ivanov, N. See & SRC Collaboration, submitted by K. Aniol

4.3.1 Introduction

Experiments E07006 and E08009 ran in February, March and April of 2011. Data for kinematic settings of 153 and 353 MeV/c for E08009 provide a thesis for Sophia Iqbal. In addition to these dedicated kinematic settings the Short Rangle Correlation(SRC) experiment also obtained data at kinematic settings out to 632 MeV/c which could be analyzed for the two body break up channel p + triton. These higher missing momenta data were collected using about 4 to 5 μA current but sufficient accumulated charge was measured to be able to extract cross sections beyond the original goal set for E08009. Moreover, the large acceptances of the Hall A spectrometers allowed for cross sections to be determined across a larger missing momentum range than the central value kinematic settings would suggest.

The electron spectrometer was fixed in angle and central momentum while the proton spectrometer's angles and central momenta were changed. The electron arm settings are in table 2.

incident beam energy	4.4506 GeV
electron spectrometer angle	20.3°
electron spectrometer momentum	3.602 GeV/c
Q^2	2.0 $(GeV/c)^2$
Bjorken x_b	1.24

Table 2: Electron spectrometer kinematic settings for E08009.

4.3.2 Experimental cross sections

Radiative corrections are obtained from the GEANT simulation of a p + triton final state missing energy spectrum at the spectrometer apertures. Experimental cross sections are given in table 3.

4.3.3 Theoretical cross sections

Vertex values of the incident electron's momentum at various positions within the target and the momenta of the scattered electron and ejected proton were provide to the Madrid theory group for calculation of the cross section at each event vertex in the GEANT simulation. The GEANT simulation also contains the detected electron and proton momenta at the spectrometers' apertures. In this way the vertex cross section can be associated with the missing momentum at the apertures. The GEANT simulation includes external and internal

P_{miss} (MeV/c)	153 $\theta_p = 47°$	353 $\theta_p = 38.5°$	466 $\theta_p = 33.5°$	632 $\theta_p = 29°$
25	(3.38 ± 0.52)			
75	(1.13 ± 0.17)			
125	$(3.13 \pm 0.48) \times 10^{-1}$			
175	$(7.18 \pm 0.11) \times 10^{-2}$			
225	$(1.44 \pm 0.22) \times 10^{-2}$	$(4.40 \pm 0.14) \times 10^{-3}$		
275	$(3.06 \pm 0.57) \times 10^{-3}$	$(1.27 \pm 0.03) \times 10^{-3}$		
325		$(6.11 \pm 0.14) \times 10^{-4}$		
375		$(3.57 \pm 0.88) \times 10^{-4}$		
425		$(1.44 \pm 0.59) \times 10^{-4}$	$(6.59 \pm 2.7) \times 10^{-4}$	
475			$(3.22 \pm 0.89) \times 10^{-4}$	
525			$(1.68 \pm 0.45) \times 10^{-4}$	
575			$(0.91 \pm 0.43) \times 10^{-4}$	
632				$(3.7 \pm 2.3) \times 10^{-5}$

Table 3: Cross sections for $^4He(e, e'p)^3H$ from E08009, for different kinematical settings given by the proton spectrometer central angle. Units are $nb/sr^2/MeV$.

bremsstrahlung. Theoretical cross sections integrated over the experimental acceptances for the full Madrid treatment and using the EMA treatment are in tables 4 and 5. Plots of the data for the two theoretical treatments are shown in figures 24 and 25.

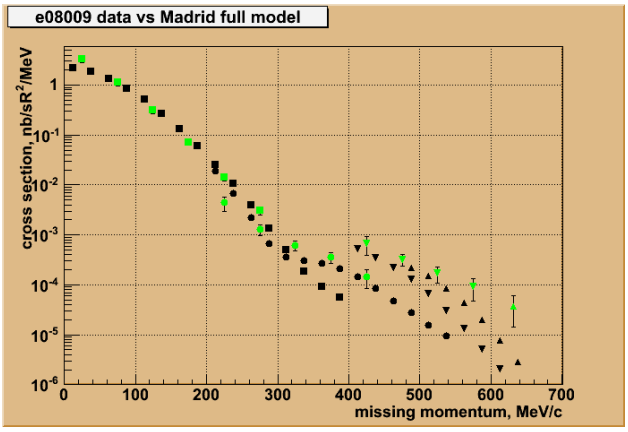

Figure 24: E08009 Data in green compared to full Madrid theoretical calculations in black. Squares are for the 153 MeV/c setting, circles are for 353 MeV/c setting, inverted triangles are for the 466 MeV/c setting and triangles are for the 632 MeV/c setting.

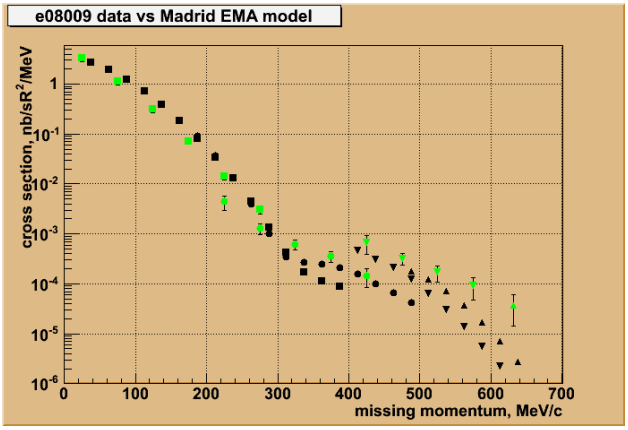

Figure 25: E08009 Data in green compared to EMA Madrid theoretical calculations in black. Squares are for the 153 MeV/c setting, circles are for 353 MeV/c setting, inverted triangles are for the 466 MeV/c setting and triangles are for the 632 MeV/c setting.

P_{miss} (MeV/c)	153 $\theta_p = 47°$	353 $\theta_p = 38.5°$	466 $\theta_p = 33.5°$	632 $\theta_p = 29°$
12.5	2.20585	0	0	0
37.5	1.82871	0	0	0
62.5	1.31389	0	0	0
87.5	0.851553	0	0	0
112.5	0.506994	0	0	0
137.5	0.26989	0	0	0
162.5	0.131086	0	0	0
187.5	0.0598725	0	0	0
212.5	0.0258303	0.0191822	0	0
237.5	0.010439	0.0067236	0	0
262.5	0.00395091	0.00220872	0	0
287.5	0.00137024	0.000668576	0	0
312.5	0.000490056	0.000357781	0	0
337.5	0.000185816	0.000309488	0	0
362.5	9.30929e-05	0.00026867	0	0
387.5	5.63916e-05	0.000207743	0	0
412.5	0	0.000141879	0.000528339	0
437.5	0	8.3657e-05	0.000340153	0
462.5	0	4.80785e-05	0.000222462	0
487.5	0	2.73925e-05	0.000126155	0.0002206
512.5	0	1.54183e-05	6.54197e-05	0.0001491
537.5	0	9.47828e-06	2.97952e-05	8.585e-05
562.5	0	0	1.28925e-05	4.4e-05
587.5	0	0	5.07677e-06	1.977e-05
612.5	0	0	2.00828e-06	7.741e-06
637.5	0	0	8.3571e-07	2.834e-06

Table 4: Madrid full theoretical cross sections integrated over the experimental acceptances for $^4He(e,e'p)^3H$ for E08009, for different kinematical settings given by the proton spectrometer central angle. Units are $nb/sr^2/MeV$.

P_{miss} (MeV/c)	153 $\theta_p = 47°$	353 $\theta_p = 38.5°$	466 $\theta_p = 33.5°$	632 $\theta_p = 29°$
12.5	0	0	0	0
37.5	2.681	0	0	0
62.5	1.916	0	0	0
87.5	1.235	0	0	0
112.5	0.729652	0	0	0
137.5	0.383898	0	0	0
162.5	0.183412	0	0	0
187.5	0.0815901	0.0903122	0	0
212.5	0.0338215	0.0362774	0	0
237.5	0.0128213	0.0129471	0	0
262.5	0.00443289	0.0039332	0	0
287.5	0.00136237	0.000998639	0	0
312.5	0.000431068	0.000342315	0	0
337.5	0.000170451	0.000264277	0	0
362.5	0.000112972	0.00024869	0	0
387.5	8.81671e-05	0.00020829	0	0
412.5	0	0.000154708	0.000455009	0
437.5	0	9.85333e-05	0.000308199	0
462.5	0	6.48162e-05	0.000206383	0
487.5	0	4.26083e-05	0.000120555	0.0001778
512.5	0	0	6.4348e-05	0.0001215
537.5	0	0	3.03616e-05	7.084e-05
562.5	0	0	1.35952e-05	3.702e-05
587.5	0	0	5.52707e-06	1.717e-05
612.5	0	0	2.25103e-06	7.01e-06
637.5	0	0	9.48271e-07	2.695e-06

Table 5: Madrid EMA theoretical cross sections integrated over the experimental acceptances for $^4He(e,e'p)^3H$ for E08009, for different kinematical settings given by the proton spectrometer central angle. Units are $nb/sr^2/MeV$.

4.4 E08027: A Measurement of G_2^P and the longitudinal-transverse spin polarizability

contributed by P. Zhu (USTC) for the E08-027 collaboration.

4.4.1 Motivation

Nucleon structure is described by the structure functions extracted from inclusive cross sections. In unpolarized case, there are two structure functions, F_1 and F_2. If the beam and target are polarized, there are two additional spin-dependent structure functions, g_1 and g_2. The g_1 structure function represents the charge-weighted quark helicity distributions at the Bjorken limit. However, g_2 has no simple interpretation in the naive parton model. It is related to the higher-twist effects, i.e., quark-gluon correlations. Measurements of the spin structure function (SSF) g_2 for the proton at low Q^2 are lacking. Currently the lowest momentum transfer investigated is $1.3\,GeV^2$ by the RSS collaboration [**?**].

The goal of this experiment is to measure the g_2 structure function for the proton at low Q^2. A measurement of the longitudinally-transverse spin polarizability (δ_{LT}) is expected to be a good test of Chiral Perturbation Theory (χPT) since it is insensitive to the $\pi - \Delta$ contribution, which is usually the main high-order correction [**?**]. The recent δ_{LT} data for the neutron indicates a significant disagreement with the χPT calculations [**?**]. However, the δ_{LT} data for the proton at low Q^2 does not exist yet. The g_2 data can provide a test of the Burkhardt-Cottingham sum rule. The low Q^2 g_2 data will help improve the precision in the hyperfine splitting of the hydrogen ground state, since the leading uncertainty in the measurement of the hyperfine splitting in the hydrogen ground state comes from the proton structure correction [**?**]. The data from this experiment may also help to improve the precision of the measurement for the proton charge radius.

4.4.2 The Experiment

The experiment successfully collected data from March to May, 2012. A measurement of the scattered electrons in the reaction $\overrightarrow{p}(\overrightarrow{e}, e')X$ at a scattering-angle of 5.69° in the low Q^2 region of $0.02 < Q^2 < 0.2\,GeV^2$ was performed to obtain the proton spin-dependent cross sections (see figure 26).

A polarized NH_3 target operating at 1 K was used as the proton target. The Dynamic Nuclear Polarization(DNP) process was used to polarize the solid NH_3 target. To avoid too much depolarization of the target, beam current was limited to $50-100$ nA during the experiment. Since the existing beam current monitors (BCMs), beam position monitors (BPMs) and calibration methods did not work at such a low current range, new BPM and BCM receivers were designed and used for low current condition. A pair of super-harps and a tungsten calorimeter were installed to calibrate the BPMs and BCMs. To compensate for the effect of the 2.5/5 T transverse target magnet field, two chicane dipole magnets were

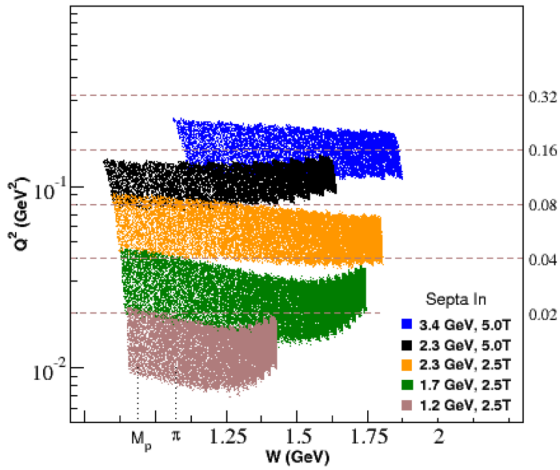

Figure 26: Kinematic coverage during the experimental run period. The numbers next to the vertical axis on the right side are the constant Q^2 values where the moments of the g_2 will be extracted.

installed. A pair of slow rasters were installed for the first time in Hall A to spread the beam to a diameter of 2 cm, combining with a pair of fast rasters. To allow detection of scattered elections at a 5.69° scattering angle, the target was installed at 876.93mm upstream from the pivot and a pair of septum magnets were installed. A new scintillator detector was developed and placed near the target to monitor the polarization of the beam and target. The instruments used in the experiment are shown in figure 27.

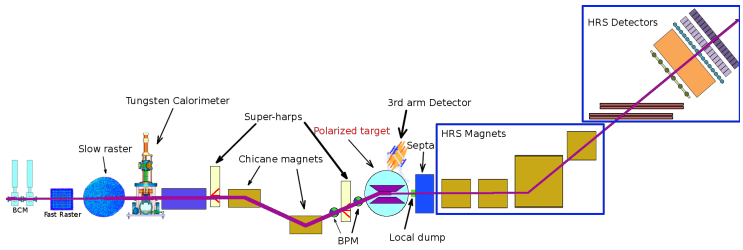

Figure 27: Installation of the g_2^p experiment.

4.4.3 Experimental Progress

The target polarization was measured by the method of Nuclear Magnetic Resonance (NMR). Thermal equilibrium measurements were used for calibrating the readout from NMR. The average measured polarization for the 5T magnet field

is 70%, while for the 2.5T magnetic field is 15% . A NIM paper was published for the g_2^p target system [**?**].

The standard HRS detectors had a good performance during the experiment. We obtained higher than 99% efficiency for the spectrumeter detectors during experiment, including track efficiency with carefully examined multitrack-events, Cherencov efficiency, lead glass calorimeter efficiency, and S1 and S2m trigger scintillator efficiency. Also the pion contamination was contained to below 0.4% with the particle identification cuts.

The beam position and angle are used for calculating the scattering angle and optimizing the optics result. Pedestals of the BPMs varied significantly during the experiment. A data base was set up to track the variation of the pedestals with time. A 2-Hz software filter was used to improve the signal/noise ratio. A new method to analyze the data of BPMs and harps, which was optimized for low beam current and large raster size, was developed. In order to transport the position from two BPMs to the target, several transport functions are fitted by using the simulation with the known target-magnetic field map.

Because of the low pass filter used in the BPM receiver and the time delay of the BPM readout, the BPM information is not enough to get the beam position event-by-event. To get the position and angle event-by-event, the raster magnet current information is used to account for the beam motion caused by the rasters. A calibrated conversion factor is needed to convert the raster current to beam position shift. For the slow raster, a carbon hole was used to convert the raster current to the size of the beam spot, while for the fast raster, the beam spot size at the calibrated BPMs was used. Since the distance of two BPMs is only 26.5 cm, while the distance of the 2nd BPM to the target is 69 cm, the uncertainty of the beam position at the target is magnified by a factor of 5. The uncertainty at the target is 1-2 mm for position and 1-2 mrad for angle.

A new Monte-Carlo simulation package was developed to study the spectrometer acceptance and the optics calibration with the target field. It has been tuned to work with the affect of the target and septum fields. The package was developed with an optimized Runge-Kutta method with self-adjusting step length to improve the speed and accuracy, based on the hall A Single Arm Monte-Carlo (SAMC) package. Several different cross-section models and energy-loss models are included in the elastic and resonance kinematic regions. The simulation results are also used to compare with the results in the packing fraction study.

The purpose of the HRS optics study is to reconstruct the kinematic variables of the scattered electrons at the reaction point. Currently, the optics data with no target field has been optimized for both the left and right HRS, which allows us to remove the additional complexity of the target field and focus on the septa and HRS magnets. The θ, ϕ and δ related optics matrix elements are calibrated with the standard sieve slit method [**?**]. At the very forward scattering angle of 5.69°, foil targets with a large z position separation are needed to calibrate the y_{tg} related optics matrix elements. A single foil carbon target and the aluminum entrance window of the target chamber are used for this purpose. This will make

the resolutions slightly worse but still satisfy our requirement. The resolutions are close to the nominal performance of the HRS system as shown in table 6.

RMS	LHRS	RHRS	Nominal performance [**?**]
δ[dp]	1.5×10^{-4}	2.4×10^{-4}	1.1×10^{-4}
θ[out of plane angle]	1.59 mrad	1.57 mrad	2.55 mrad
y	3.3 mm	2.9 mm	1.7 mm
ϕ[in plane angle]	0.99 mrad	0.82 mrad	0.85 mrad

Table 6: Performance summary of RMS values for optics study without target field

In g_2^p setting, the strong transverse target field makes the optics study more challenging. To deal with this target field, the reconstruction process is separated into two parts. The first part, containing the septum magnet and HRS, is assumed to be represented by the matrix with no target field which has been described above. Unfortunately, the configuration changes during the experiment because of the broken septum magnet, which requires the matrix elements to be re-calibrated. The simulation package mentioned above is used to calculate the reference angles of the fits for the recalibration. The second part, the target field region, is treated only with a ray-tracing method. The same simulation package is also used here to calculate the trajectory of the scattered electrons. The calibration has been completed for LHRS and will be done soon for RHRS.

In additional to the calibration of the optics matrix, the central angle of the spectrometer system is studied with two different methods: using survey information or using double elastic peaks [**?**]. The survey information provides smaller systematic uncertainty and is the one being used. The central angle, together with the relative scattering angle reconstructed by the optics matrix, is used to calculate the scattering angle of the out-going electrons.

In addition, an acceptance study is underway. A correction was made to the SNAKE model to match data at focal plane well in good septum situation (figure 28). With this updated SNAKE model, forward and reverse transport functions

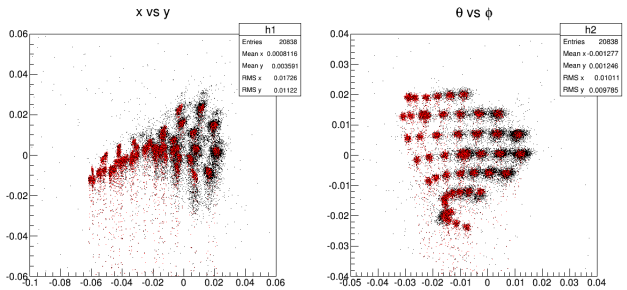

Figure 28: Match in focal plane for acceptance study

have been fitted to describe the electron trajectories from the target plane to the

focal plane (without target field). These functions have been incorporated into the simulation package. The acceptance for the other septum configurations will be studied soon.

The NH_3 target cell is comprised of ammonia beads and liquid helium. The packing fraction, or the ratio of the length of ammonia to the total target length, must be understood for dilution analysis. To extract the packing fraction, the elastic yields are compared from a production run and a "dummy" run, where the target cell is filled only with liquid helium. Currently, the fitting routine is being optimized to remove contamination to the elastic peak from the quasi-elastic peak. The packing fraction from one of our setting is 0.6.

The measured asymmetry is diluted by contributions from the nitrogen in the ammonia target material, helium used to cool the target, and the aluminum target end caps. This contamination is removed, giving us a true proton asymmetry, using a dilution factor analysis, which accounts for scattering from the unpolarized material. The aluminum and helium background is determined from experimental data, but the nitrogen background is more complicated since we do not have pure nitrogen data (we only took data on a carbon target). Since the Small Angle GDH experiment has similar kinematics to g2p, we can use the saGDH nitrogen data set to tune the Bosted model for use at the g2p kinematics. Elastic and inelastic radiative corrections have been completed on the saGDH nitrogen data and the Bosted model has been tuned to $\pm 5\%$ level [**?**]. The actual nitrogen background is scaled by using the tuned Bosted model with the g2p carbon data. Figure 29 shows the dilution factor for one of our kinematic settings.

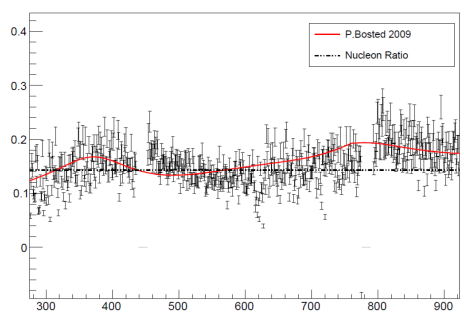

Figure 29: Dilution factor for the 3.35GeV beam energy, 5T transverse field setting; x axis is $\nu(MeV)$

Once the acceptance study, the packing fraction and the dilution studies are complete, the physics asymmetries and the cross sections can be extracted. Preliminary results are expected in another year or so.

5 Publications

Publications published during 2014, either in preprint or finally, based on experiments run in Hall A of Jefferson Lab.

1. C J Horowitz *et al.*, A way forward in the study of the symmetry energy: experiment, theory, and observation, J. Phys. G: Nucl. Part. Phys. 41 (2014) 093001

2. S. Golge, B. Vlahovic, B. Wojtsekhowski, High-intensity positron microprobe at the Thomas Jefferson National Accelerator Facility, J. Appl. Phys. 115, 234907 (2014)

3. A. Camsonne *et al.*, JLab Measurement of the ^{4}He Charge Form Factor at Large Momentum Transfers, Phys. Rev. Lett. 112, 132503 (2014)

4. M. Mihovilovič *et al.*, Measurement of Double-Polarization Asymmetries in the Quasielastic ^{3}He(e,ed) Process, Phys. Rev. Lett. 113, 232505 (2014)

5. The Jefferson Lab PVDIS Collaboration, Measurement of parity violation in electronquark scattering, Nature 506, 6770 (06 February 2014)

6. Y. Zhang *et al.*, Measurement of pretzelosity asymmetry of charged pion production in semi-inclusive deep inelastic scattering on a polarized He3 target, Phys. Rev. C 90, 055209 (2014)

7. P Monaghan *et al.*, Measurement of the ^{12}C(e,ep)11B two-body breakup reaction at high missing momentum, J. Phys. G: Nucl. Part. Phys. 41 (2014) 105109

8. J. Katich *et al.*, Measurement of the Target-Normal Single-Spin Asymmetry in Deep-Inelastic Scattering from the Reaction ^{3}He$^\uparrow$(e,e)X, Phys. Rev. Lett. 113, 022502 (2014)

9. O. Hen *et al.*, Momentum sharing in imbalanced Fermi systems, Science 346, 614 (2014)

10. M. Posik *et al.*, Precision Measurement of the Neutron Twist-3 Matrix Element d_2^n: Probing Color Forces, Phys. Rev. Lett. 113, 022002

11. Igor Korover *et al.*, Probing the Repulsive Core of the Nucleon-Nucleon Interaction via the ^{4}He(e,epN) Triple-Coincidence Reaction, Phys. Rev. Lett. 113, 022501 (2014)

12. Y. X. Zhao *et al.*, Single Spin Asymmetries in Charged Kaon Production from Semi-Inclusive Deep Inelastic Scattering on a Transversely Polarized ^{3}He Target, Phys. Rev. C.90.055201, 2014

13. K. Allada *et al.*, Single spin asymmetries of inclusive hadrons produced in electron scattering from a transversely polarized ^{3}He target, Phys. Rev. C 89, 042201(R), 2014

14. Simona Malace, David Gaskell, Douglas W. Higinbotham, Ian Cloet, The Challenge of the EMC Effect: existing data and future directions, Int. J. Mod. Phys. E 23 (2014) 1430013

15. Krishna S. Kumar *et al.*, The MOLLER Experiment: An Ultra-Precise Measurement of the Weak Mixing Angle using Møller Scattering, arxiv:1411.4088

16. B. Wojtsekhowski *et al.*, On measurement of the isotropy of the speed of light, arxiv:1409.6373

17. Douglas W. Higinbotham, Or Hen, Comment on "Measurement of 2- and 3-nucleon short range correlation probabilities in nuclei", arxiv:1409.3069

18. D. S. Parno *et al.*, Precision Measurements of A_1^n in the Deep Inelastic Regime, arxiv:1406.1207

6 Theses

1. *Measurement of the photon electroproduction cross section at JLAB with the goal of performing a Rosenbluth separation of the DVCS contribution*
   Alejandro Marti Jimenez-Arguello
   https://misportal.jlab.org/ul/publications/view_pub.cfm?pub_id=13562

2. *A Precision Measurement of the Neutron D2: Probing the Color Force*
   Matthew Posik
   https://misportal.jlab.org/ul/publications/view_pub.cfm?pub_id=13193

7 Hall A Collaboration Member List, 2014

Argonne National Lab
John Arrington
Paul Reimer
Xiaohui Zhan

Brookhaven National Lab
Xin Qian

Budker Institute of Nuclear Physics
Dima Nikolenko
Igor Rachek

Cairo University
Hassan Ibrahim

California State University
Konrad A. Aniol
Martin B. Epstein
Dimitri Margaziotis

Carnegie Mellon University
Gregg Franklin
Vahe Mamyan
Brian Quinn

The Catholic University of America
Marco Carmignotto
Tanja Horn
Indra Sapkota

Commissariat a lEnergie Atomique - Saclay
Maxime Defurne
Nicole d'Hose
Eric Fuchey
Franck Sabatie

China Institute of Atomic Energy (CIAE)
Xiaomei Li
Shuhua Zhou

Christopher Newport University
Ed Brash

College of William and Mary
David S. Armstrong
Carlos Ayerbe Gayoso
Todd Averett
Juan Carlos Cornejo
Melissa Cummings
Wouter Deconinck
Keith Griffioen
Joe Katich
Charles Perdrisat
Yang Wang
Huan Yao
Bo Zhao

Duquesne University
Fatiha Benmokhtar

Duke University
Steve Churchwell
Haiyan Gao
Calvin Howell
Min Huang
Richard Walter
Qiujian Ye

Faculte des Sciences de Monastir (Tunisia)
Malek Mazouz

Florida International University
Armando Acha
Werner Boeglin
Luminiya Coman
Marius Coman
Lei Guo
Hari Khanal
Laird Kramer
Pete Markowitz
Brian Raue
Jeorg Reinhold

Forschungszentrum Rossendorf Institut für Kern- und. Hadronenphysik
Frank Dohrmann

Gesellschaft fur Schwerionenforschung (GSI)
Javier Rodriguez Vignote

Hampton University
Eric Christy
Leon Cole
Peter Monaghan

Harvard University
Richard Wilson

Hebrew University of Jerusalem
Moshe Friedman
Aidan Kelleher
Guy Ron

Huangshan University
Hai-jiang Lu
XinHu Yan

Idaho State University
Mahbub Khandaker

Dustin McNulty

INFN/Bari
Raffaele de Leo

INFN/Catania
Antonio Guisa
Francesco Mammolit
Giuseppe Russo
Concetta Maria Sutera

INFN/Lecce
Roberto Perrino

INFN/Roma
Marco Capogni
Evaristo Cisbani
Francesco Cusanno
Fulvio De Persio
Alessio Del Dotto
Cristiano Fanelli
Salvatore Frullani
Franco Garibaldi
Franco Meddi
Guido Maria Urciuoli

Institute of Modern Physics, Chinese Academy of Sciences
Xurong Chen

Institut de Physique Nucleaire - Orsay
Camille Desnault
Alejandro Marti Jimenez-Arguello
Carlos Munoz Camacho
Rafayel Paremuzyan

ISN Grenoble
Eric Voutier

James Madison University
Gabriel Niculescu
Ioana Niculescu

Jefferson Lab
Alexandre Camsonne
Larry Cardman
Jian-Ping Chen
Eugene Chudakov
Mark Dalton
Kees de Jager
Alexandre Deur
Ed Folts
David Gaskell
Javier Gomez
Ole Hansen
Douglas Higinbotham
Mark K. Jones
Thia Keppel
John Lerose
Simona Malace
Bert Manzlak
David Meekins
Robert Michaels
Bryan Moffit
Sirish Nanda
Noel Okay
Lubomir Pentchev
Yi Qiang
Lester Richardson
Yves Roblin
Brad Sawatzky
Jack Segal
Dennis Skopik
Patricia Solvignon
Mark Stevens
Riad Suleiman
Stephanie Tysor
Bogdan Wojtsekowski
Jixie Zhang

Jozef Stefan Institute
Miha Mihovilovic
Simon Sirca

Kent State University
Bryon Anderson
Mina Katramatou
Elena Khrosinkova
Richard Madey
Mark Manley
Gerassimos G. Petratos
Larry Selvey
John Watson

Kharkov Institute of Physics and Technology
Oleksandr Glamazdin
Viktor Gorbenko
Roman Pomatsalyuk
Vadym Vereshchaka

Kharkov State University
Pavel Sorokin

Khalifa University
Issam Qattan

Lanzhou University
Bitao Hu
Yi Zhang

Longwood University
Tim Holmstrom
Keith Rider
Jeremy St. John
Vincent Sulkosky
Wolfgang Troth

Los Alamos Laboratory
Jin Huang
Xiaodong Jiang
Ming Xiong Liu

LPC Clermont-Ferrand France
Pierre Bertin
Helene Fonvielle

Mississippi State University

Dipangkar Dutta
Mitra Shabestari
Amrendra Narayan
Nuruzzaman

Massachusetts Institute of Technology
Kalyan Allada
Bill Bertozzi
Shalev Gilad
Navaphon "Tai" Muangma
Kai Pan
Cesar Fernandez Ramirez
Rupesh Silwal

Mountain View Collage
Ramesh Subedi

Negev Nuclear Research Center
Arie Beck
Sharon Beck

NIKHEF
Jeff Templon

Norfolk State University
Wendy Hinton
Vina Punjabi

North Carolina Central University
Benjamin Crowe
Branislav (Branko) Vlahovic

North Carolina A&T State University
Ashot Gasparian

Northwestern University
Ralph Segel

Ohio University
Mongi Dlamini
Norman Israel
Paul King
Julie Roche

Old Dominion University
S. Lee Allison
Gagik Gavalian
Mohamed Hafez
Charles Hyde
Kijun Park
Hashir Rashad
Larry Weinstein

Peterburg Nuclear Physics Institute
Viacheslav Kuznetsov

Regina University
Alexander Kozlov
Andrei Semenov

Rutgers University
Lamiaa El Fassi
Ron Gilman
Gerfried Kumbartzki
Katherine Myers
Ronald Ransome
Yawei Zhang

Saint Norbert College
Michael Olson

Seoul National University
Seonho Choi
Byungwuek Lee

Smith College
Piotr Decowski

St Mary's University
Davis Anez
Adam Sarty

Stony Brook University
Rouven Essig

Syracuse University
Zafar Ahmed
Richard Holmes
Paul A. Souder

Technische Universität München
Jaideep Singh

Tel Aviv University
Nathaniel Bubis
Or Chen
Igor Korover
Jechiel Lichtenstadt
Eli Piasetzky
Ishay Pomerantz
Ran Shneor
Israel Yaron

Temple University
David Flay
Zein-Eddine Meziani
Michael Paolone
Matthew Posik
Nikos Sparveris

Tohoku University
Kouichi Kino
Kazushige Maeda
Teijiro Saito
Tatsuo Terasawa
H. Tsubota

Tsinghua University
Zhigang Xiao

Universidad Complutense de Madrid (UCM)
Joaquin Lopez Herraiz
Luis Mario Fraile

Maria Christina Martinez Perez
Jose Udias Moinelo

University of Connecticut
Andrew Puckett

Universitat Pavia
Sigfrido Boffi

University "La Sapienza" of Rome
Cristiano Fanelli
Fulvio De Persio

University of Glasgow
John Annand
David Hamilton
Dave Ireland
Ken Livingston
Dan Protopopescu
Guenther Rosner
Johan Sjoegren

University of Illinois
Ting Chang
Areg Danagoulian
J.C. Peng
Mike Roedelbronn
Youcai Wang
Lindgyan Zhu

University of Kentucky
Dan Dale
Tim Gorringe
Wolfgang Korsch

University of Lund
Kevin Fissum

University of Manitoba
Juliette Mammei

University of Maryland
Elizabeth Beise

University of Massachusetts, Amherst
Krishna S. Kumar
Seamus Riordan
Jon Wexler

University of New Hampshire
Toby Badman
Trevor Bielarski
John Calarco
Bill Hersman
Maurik Holtrop
Donahy John
Mark Leuschner
Elena Long
James Maxwell
Sarah Phillips
Karl Slifer
Timothy Smith
Ryan Zielinski

University of Regina
Garth Huber
George Lolos
Zisia Papandreou

University of Saskatchewan
Ru Igarashi

University of Science and Technology of China (USTC)
Yi Jiang
Wenbiao Yan
Yunxiu Ye
Zhengguo Zhao
Yuxian Zhao
Pengjia Zhu

University of South Carolina
Steffen Strauch

University of Tennessee
Nadia Fomin

University of Virginia
Khem Chirapatpimol
Donal Day
Xiaoyan Deng
Gordon D. Gates
Gu Chao
Charles Hanretty
Ge Jin
Richard Lindgren
Jie Liu
Nilanga Liyanage
Vladimir Nelyubin
Blaine Norum
Kent Paschke
Peng Chao
Oscar Rondon
Kiadtisak Saenboonruang
William "Al" Tobias
Diancheng Wang
Kebin Wang
Zhihong Yi
Zhiwen Zhao
Xiaochao Zheng
Jiayao Zhou

University of Washington
Diana Parno

Yamagata University
Seigo Kato
Hiroaki Ueno

Yerevan Physics Institute
Sergey Abrahamyan
Nerses Gevorgyan
Edik Hovhannisyan

Armen Ketikyan
Samvel Mayilyan
Karen Ohanyan
Artush Petrosyan
Galust Sargsyan
Albert Shahinyan
Hakob Voskanian

Inactive Members
Mattias Anderson
Maud Baylac
Hachemi Benaoum
J. Berthot
Michel Bernard
Louis Bimbot
Tim Black
Alexander Borissov
Vincent Breton
Herbert Breuer
Etienne Burtin
Christian Cavata
George Chang
Nicholas Chant
Jean-Eric Ducret
Zhengwei Chai
Brandon Craver
Natalie Degrande
Rachel di Salvo
Pibero Djawotho
Chiranjib Dutta
Kim Egiyan
Stephanie Escoffier
Catherine Ferdi
Megan Friend
Robert Feuerbach
Mike Finn
Bernard Frois
Oliver Gayou
Charles Glashausser
Jackie Glister
Greg Hadcock
Brian Hahn
Harry Holmgren
Sebastian Incerti
Mauro Iodice
Riccardo Iommi
Florian Itard
Stephanie Jaminion
Steffen Jensen
Sudirukkuge Tharanga Jinasundera
Cathleen Jones
Lisa Kaufman
James D. Kellie
Sophie Kerhoas
Ameya Kolarkar
Norm Kolb
Ioannis Kominis
Serge Kox
Kevin Kramer
Elena Kuchina
Serguei Kuleshov
Jeff Lachniet
Geraud Lavessiere
Antonio Leone
David Lhuillier
Meihua Liang
Han Liu
Robert Lourie
Jacques Marroncle
Jacques Martino
Kathy McCormick
Justin McIntyre
Luis Mercado
Brian Milbrath
Wilson Miller
Joseph Mitchell
Jean Mougey
Pierre Moussiegt
Alan Nathan
Damien Neyret
Stephane Platchkov
Thierry Pussieux
Gilles Quemener
Abdurahim Rakhman
Bodo Reitz
Rikki Roche
Philip Roos
David Rowntree
Gary Rutledge
Marat Rvachev
Arun Saha
Neil Thompson
Luminita Todor
Paul Ulmer
Antonin Vacheret
Luc Van de Hoorebeke
Robert Van de Vyver
Pascal Vernin
Dan Watts
Krishni Wijesooriya
Hong Xiang
Wang Xu
Jingdong Yuan
Jianguo Zhao
Jingdong Zhou
Xiaofeng Zhu
Piotr Zolnierczuk